Prior Learning in Introspective VAEs

Anonymous authors
Paper under double-blind review

Abstract

Variational Autoencoders (VAEs) are a popular framework for unsupervised learning and data generation. A plethora of methods have been proposed focusing on improving VAEs, with the incorporation of adversarial objectives and the integration of prior learning mechanisms being prominent directions. When it comes to the former, an indicative instance is the recently introduced family of Introspective VAEs aiming at ensuring that a low likelihood is assigned to unrealistic samples. In this study, we focus on the Soft-IntroVAE (S-IntroVAE) and investigate the implication of incorporating a multimodal and learnable prior into this framework. Namely, we formulate the prior as a third player and show that when trained in cooperation with the decoder constitutes an effective way for prior learning, which shares the Nash Equilibrium with the vanilla S-IntroVAE. Furthermore, based on a modified formulation of the optimal ELBO in S-IntroVAE, we develop theoretically motivated regularizations, namely (i) adaptive variance clipping to stabilize training when learning the prior and (ii) responsibility regularization to discourage the formation of inactive prior mode. Finally, we perform a series of targeted experiments on a 2D density estimation benchmark and in an image generation setting comprised of the (F)-MNIST and CIFAR-10 datasets demonstrating the benefit of prior learning in S-IntroVAE in generation and representation learning.

1 Introduction

Variational Autoencoders (VAEs) (Kingma & Welling, 2013; Rezende et al., 2014) constitute a popular generative framework where variational inference is utilized to learn low-dimensional embeddings by modeling the density of the high-dimensional data. VAEs enjoy a plethora of applications, ranging from anomaly detection (Chauhan et al., 2022) to representation disentanglement (Higgins et al., 2016) and high-resolution image generation (Razavi et al., 2019). Despite VAEs falling short of other popular generative paradigms, such as the Generative Adversarial Networks (GANs) (Goodfellow et al., 2020) and Diffusion models (Ho et al., 2020) in terms of generation quality, they are distinctive in the sense of simultaneously providing the amortized inference and generation modeling (Gatopoulos & Tomczak, 2021).

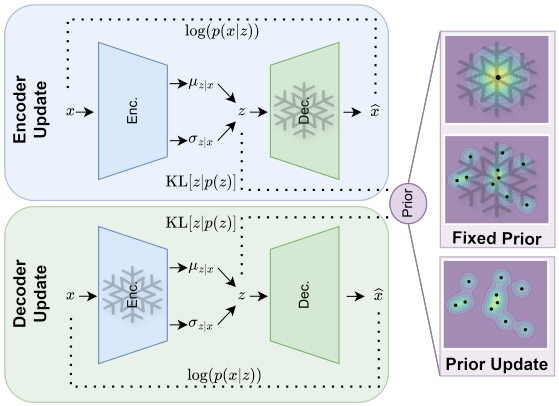

Figure 1: Prior player realizations within Introspective VAEs. The prior component can be regarded as a third player that can actively participate in the adversarial game along with the encoder and the decoder. The overlayed snowflake indicates that the component is not updated.

Building upon that, combining VAEs with these frameworks has been a popular research direction aiming at retaining its merits while mitigating its limitations (Makhzani et al., 2016). With diffusion models emerging as the state-of-the-art framework for image synthesis (Yang et al., 2022), there are recent works on VAE/diffusion hybrids (Preechakul et al., 2022; Rey et al., 2019). Additionally, the VAE/GAN hybrid literature is also an established sub-field targeted at improving the poor training stability of GANs (Mescheder et al., 2018) and generation diversity (Huang et al.,

2018) while addressing the blurry generation of VAEs. Another independent direction to improving VAEs is learning a more flexible prior as opposed to fitting into a fixed one, commonly the standard Gaussian. Flexible priors allow for identifying structure within the data which is of high interest in the unsupervised and semi-supervised learning setups. Moreover, sufficiently expressive priors are needed for generating realistic data from complex distributions (Lavda et al., 2019; Dilokthanakul et al., 2016). Additionally, utilizing the structured capture in the latent space (Lavda et al., 2019) can benefit the generation performance as well as provide control over the semantics of the generated samples even in the absence of labels.

Motivated by the prospect of combining the strength of two distinct and conceptually different directions for enhancing VAEs, we consider the problem of incorporating prior learning in the S-IntroVAE framework. Our intuition is that the appealing features of reducing over-regularization and holes as enabled by prior learning are not sufficient for realistic sample generation. On the other hand, although adversarially trained VAEs possess higher quality generation capabilities, they are still subject to the problem associated with assuming an over-simplistic prior.

Based on these, we formulate the prior as an additional player in S-IntroVAE which participates in the adversarial training. More specifically, we extend the original analysis provided by Daniel & Tamar (2021) and conclude that the prior–decoder cooperation scheme is a viable option for learning the prior while remaining faithful to the Nash Equilibrium (NE) of the vanilla S-IntroVAE. Our work is partly related to the CS-IntroVAE (Yu et al., 2023) where a fixed 3-component Mixture of Gaussian (MoG) was integrated into S-IntroVAE by replacing the Kullback–Leibler (KL) with the Cauchy–Schwarz divergence to allow for closed-form divergence computation. Notably, in our work, we follow the original variational analysis provided in (Daniel & Tamar, 2021), using the KL divergence and its theoretical properties, thereby investigating the effect of using a multimodal prior, including its learnable form, in isolation.

Formally our contributions are:

- extending the original S-IntroVAE under the prior–decoder cooperation scheme.
- two theoretically motivated regularizations (i) adaptive variance clipping and (ii) responsibilities entropy which enable robust prior–learning cooperation.
- the experiments on a synthetic 2D density estimation and an image generation task demonstrating the benefit of prior learning in S-IntroVAE in generation and representation learning.

2 Related Work

VAEs: In VAEs (Kingma & Welling, 2013; Rezende et al., 2014) an autoencoder-based structure is utilized, along with variational inference, to maximize a lower bound on the marginal log-likelihood of the data (the evidence lower bound, ELBO). More specifically, this resorts to simultaneously minimizing the sum of the empirical reconstruction error and the Kullback–Leibler (KL) divergence between the extracted latent representations and an assumed prior (typically the standard Gaussian distribution). A tighter ELBO was proposed by Burda et al. (2015), based on an importance weighting scheme, providing more flexibility during training by being more forgiving of inaccurate posterior estimates. Hierarchical variations of VAEs (Sønderby et al., 2016; Vahdat & Kautz, 2020) rely on multiple stochastic layers where each of them is conditioned on the previous one, resulting in more efficient representation learning (Zhao et al., 2017; Child, 2020).

Prior Assumption in VAEs: Several studies suggest that assuming an over-simplistic prior can over-regularize the VAEs hindering their performance (Hoffman & Johnson, 2016; Lin & Clark, 2020; Tomczak & Welling, 2018). Goyal et al. (2017) argue that assuming a standard Gaussian prior can omit meaningful semantic information in the latent representation. Moreover an over-simplistic prior introduces holes in the prior negatively affecting the generation capabilities of VAEs (Aneja et al., 2021; Rezende & Viola, 2018). Towards addressing this shortcoming, Tomczak & Welling (2018) proposed the VampPrior where trainable pseudo-inputs are fed into the encoder providing the parameters of a MoG distribution to replace the standard one. Connor et al. (2021) adopt a manifold-learning approach to define an MoG prior, which is better crafted for the latent space of the data. Kalatzis et al. (2020) assume a Riemannian latent space where the prior is inferred from the data, replacing the standard Gaussian with a Brownian motion prior.

Adversarial Objectives in VAEs: In Adversarial Autoencoders (AEEs) (Makhzani et al., 2016) the latent space is regularized into following the assumed prior through a min-max game between the encoder and a discriminator module. The VAE/GAN hybrid was proposed by Larsen et al. (2016) where the similarity distance, for measuring the reconstruction error, is implicitly learned through an adversarial game in which the decoder network serves as both a VAE decoder and the generator of a GAN. In the seminal IntroVAE (Huang et al., 2018), the VAEs are framed as an adversarial game between the encoder and the decoder by considering the KL divergence as an energy function. The S-IntroVAE (Daniel & Tamar, 2021) improves the training stability of IntroVAE, while also providing the theoretical analysis suggesting that introspective VAEs constitute a variational instance of GANs. In CS-IntroVAE (Yu et al., 2023) the KL was replaced by Cauchy–Schwarz divergence while using a fixed three-component MoG in S-IntroVAE leading to improved generation performance.

3 Background

Our work builds upon the framework proposed by Daniel & Tamar (2021). To avoid confusion we adopt, whenever possible, identical notations as presented in their work. Let $x \sim p_{\text{data}}(x)$ be a data sample and z its latent representation. A VAE aims at learning a parametric model $p_{d_\theta}(x, z) = p_{d_\theta}(x|z)p_z(z)$ such that the marginal log-likelihood of the data is maximized. Due to the intractability of that likelihood (Kingma & Welling, 2013), we resort to maximizing the ELBO. Assuming a prior p_z on the latent space, an encoder q_ϕ providing the approximating posterior and a decoder p_{d_θ}, parametrized by ϕ and θ respectively, we evaluate the ELBO, denoted as W, at point x as:

$$W(x; q_\phi, p_{d_\theta}) = -\,\mathrm{KL}[q_\phi(z|x)||p_z(z)] + \mathbb{E}_{z\sim q_\phi(z|x)}[\log p_{d_\theta}(x|z)] \leq \log p(x), \tag{1}$$

with $\mathrm{KL}[\cdot||\cdot]$ denoting the KL divergence. In practice, the encoder and the decoder are typically realized through neural networks with parameters ϕ and θ, respectively. The β-VAE reformulates the ELBO by weighting the relative contribution of the KL term using the β hyperparameter, that is:

$$W(x; q_\phi, p_{d_\theta}, \beta) = -\beta \cdot \mathrm{KL}[q_\phi(z|x)||p_z(z)] + \mathbb{E}_{z\sim q_\phi(z|x)}[\log p_{d_\theta}(x|z)]. \tag{2}$$

Note that, from an optimization perspective, the β-VAE ELBO formulation is equivalent to using independent weighting hyperparameters for each of its constituting terms, such that $W(x; q_\phi, p_{d_\theta}, \beta_{\text{rec}}, \beta_{\text{KL}}) = -\beta_{\text{KL}} \cdot \mathrm{KL}[q_\phi(z|x)||p(z)] + \beta_{\text{rec}} \cdot \mathbb{E}_{z\sim q_\phi(z|x)}[\log p_{d_\theta}(x|z)]$. This ELBO formulation is convenient for tuning the S-IntroVAE and therefore is the adopted ELBO formulation. Additionally, we will omit expressing the ELBO in terms of β_{KL} and β_{rec} to enhance clarity.

3.1 Learning the optimal prior

In light of the previously discussed implication of imposing a simple prior in VAE, the question arises: what is the optimal prior $p_z(z)$? In this aspect, an insightful reformulation of the empirical ELBO is provided by Tomczak (2022):

$$\begin{aligned}\mathbb{E}_{x\sim p_{\text{data}}(x)}[W(x; q_\phi, p_{d_\theta}, \beta_{\text{rec}}, \beta_{\text{KL}})] = \beta_{\text{rec}} \cdot \mathbb{E}_{x\sim p_{\text{data}}(x)}[\mathbb{E}_{z\sim q_\phi(z|x)}[\log p_{d_\theta}(x|z)] \\ + \beta_{\text{KL}} \cdot (\mathbb{H}[q_\phi(z|x)]] - \mathbb{CE}[q_\phi(z)||p_z(z)])\,,\end{aligned} \tag{3}$$

with $\mathbb{H}[\cdot]$ and $\mathbb{CE}[\cdot||\cdot]$ denoting the Shannon and the cross-entropies, respectively, and $q_\phi(z) = \mathbb{E}_{x\sim p_{\text{data}}(x)}[q_\phi(z|x)]$ is the aggregated posterior. The formulation above suggests that the optimal prior can be found as the maximizer of the ELBO, namely $p_z(z) = q_\phi(z)$, as this is when the negative cross entropy term is maximized (Gibbs' inequality). Towards this, utilizing a learnable MoG prior emerges as a relevant alternative to the standard Gaussian. A prior–encoder pairing was realized by Tomczak & Welling (2018), termed as VampPrior, leading to better separation in latent space. Formally the MoG and Vamp

M-modal priors are parametrized as:

$$p_\lambda(z) = \sum_{i=1}^{M} w_i \cdot \mathcal{N}(z|\mu_i, \sigma_i^2 I) \text{ and } p^q(z) = \sum_{i=1}^{M} w_i \cdot q_\phi(z|x_i),$$

respectively, with $\sum_{i=1}^{M} w_i = 1$ and w_i the contribution of each component, μ_i and σ_i the means and variances of the MoG prior and x_i pseudo-inputs for the VampPrior.

3.2 S-IntroVAE

In typical VAEs, the encoder and the decoder are updated simultaneously in a single backpropagation stage. Motivated by the observation that assigning a high likelihood for the real data does not necessarily imply assigning a low likelihood for the unlikely ones, the Introspective VAEs family (Huang et al., 2018; Daniel & Tamar, 2021) formulates an adversarial game between the encoder and the decoder. In S-IntroVAE (Daniel & Tamar, 2021), the ELBO is regarded as an energy function, and on that basis, the encoder is induced to assign high energy to real and low energy to generated data. On the contrary, the decoder aims at generating data (i.e. reconstructed and generated samples) that resemble those of the real data distribution to fool the encoder. The above setup constitutes an adversarial game between the encoder and the decoder similar to the GAN (Goodfellow et al., 2020) paradigm.

For notational brevity in the derivations below we drop the dependence on the parameters θ and ϕ and simply write d for the decoder and q for the encoder, while we henceforth refer to $\mathbb{E}_{x\sim p(x)}[\cdot]$ simply as $\mathbb{E}_p[\cdot]$ when clear from the context. Then, formally, given the empirical $p_{\text{data}}(x)$ and $p_d(x) = \mathbb{E}_{p_z(z)}[p_d(x|z)]$ the generated data distribution, the encoder q and decoder d are alternately updated towards maximizing their respective objectives $L_q(q,d)$ and $L_d(q,d)$ defined as:

$$\begin{aligned} L_q(q,d) &= \mathbb{E}_{p_{\text{data}}}\left[W(x;q,d)\right] - \mathbb{E}_{p_d}[\frac{1}{\alpha} \cdot \exp(\alpha W(x;q,d))], \\ L_d(q,d) &= \mathbb{E}_{p_{\text{data}}}\left[W(x;q,d)\right] + \gamma \cdot \mathbb{E}_{p_d}\left[W(x;q,d)\right], \end{aligned} \tag{4}$$

where $\alpha \geq 1$ and $\gamma \geq 0$ are hyperparameters. Daniel & Tamar (2021) show that there is a NE for this two-player game. Specifically, define d^* as:

$$d^* \in \arg\min_d \left\{\text{KL}[p_{\text{data}}(x)||p_d(x)] + \gamma \cdot \mathbb{H}[p_d(x)]\right\}. \tag{5}$$

Assumption 1 (Modified - Daniel & Tamar (2021))**.** *For all x such that $p_{data}(x) \geq 0$ we have that $[p_{d^*}(x)]^{\alpha+1} \leq p_{data}(x)$.*

Remark 1. *The assumption above is a modified version of the one used by Daniel & Tamar (2021) and essentially suggests that $p_{d^*}(x)$ has to be sufficiently enclosed by the true data distribution. We refer readers to B.1 for a detailed explanation of this matter.*

Theorem 1 (Daniel & Tamar (2021))**.** *Under the assumption 1, the pair of optimal $q^* = p_{d^*}(z|x)$ and d^* as defined in equation 5 constitutes a NE of the game equation 4.*

We refer the readers to the original work of Daniel & Tamar (2021) for the proof that for every p_{data} there always exists $\gamma \geq 0$ such that assumption 1 holds for p_{d^*}. Theorem 1 suggests that, at convergence, the S-IntroVAE formulation leads to optimal inference capabilities (i.e. the approximated posterior equals the true one) while the generated data distribution converges to an entropy-regularized version of the true data distribution.

4 Prior Learning in S-IntroVAE

Algorithm 1 Prior Learning in S-IntroVAE Daniel & Tamar (2021). The red-highlighted segments indicate the parts that differ from the standard Gaussian S-IntroVAE. The L_{rec} and the L_{KL} refer to the reconstruction loss and the KL divergence between the posterior and the prior target respectively, whereas the $L_{\text{KL}}^{\mathtt{sg}}$ is a modified KL divergence that applies the stop-gradient $\mathtt{sg}$ operator on the prior as target.

Require: $\beta_{rec}, \beta_{\text{KL}}, \beta_{neg}, \gamma$, r_{entropy}
$\phi_E, p_\Lambda, \theta_D \leftarrow$ Initialize network parameters
$s \leftarrow 1/\text{input dim}$ ▷ Scaling constant
$\gamma_r \leftarrow 10^{-8}$ ▷ Scaling parameter for fake data reconstruction

while not converged **do**
  $x_{\text{real}} \leftarrow$ Random mini-batch from dataset
  $z_s \leftarrow$ Samples from the MoG prior ▷ Log-variance clipping performed according to Eq. 10

  procedure UpdateEncoder(ϕ_E)
    $W \leftarrow -s \cdot (\beta_{\text{rec}} \cdot \text{L}_{\text{rec}}(X) + \beta_{\text{KL}} \cdot \text{L}_{\text{KL}}(X))$
    $W_f \leftarrow -s \cdot (\beta_{\text{rec}} \cdot \text{L}_{\text{rec}}(D(z_s)) + \beta_{\text{neg}} \cdot \text{L}_{\text{KL}}(D(z_s)))$
    $\exp W_f \leftarrow 0.5 \cdot \exp(2 \cdot W_f)$
    $C = \text{ComputeResponsibilities}(x_{\text{real}})$ ▷ Eq. 11
    $\text{Entropy}_C = \text{NormalizedEntropy}(C)$
    $L_E \leftarrow W - \exp W_f + s \cdot r_{\text{entropy}} \cdot \text{Entropy}_C$
    $\phi_E \leftarrow \phi_E + \eta \nabla_{\phi_E}(L_E)$ ▷ Adam update
  end procedure

  procedure UpdatePriorAndDecoder(p_Λ, θ_D)
    $W \leftarrow -s \cdot (\beta_{\text{rec}} \cdot \text{L}_{\text{rec}}(X) + \beta_{\text{KL}} \cdot \text{L}_{\text{KL}}(X))$
    $W_f \leftarrow -s \cdot (\gamma_r \cdot \beta_{\text{rec}} \cdot \text{L}_{\text{rec}}(\mathtt{sg}(D(z_s))) + \beta_{\text{KL}} \cdot \text{L}_{\text{KL}}^{\mathtt{sg}}(D(z_s)))$
    $L_{PD} \leftarrow W + \gamma \cdot W_f$
    $\theta_D \leftarrow \theta_D + \eta \cdot \nabla_{\theta_D}(L_{PD})$ ▷ Adam update
    $p_\Lambda \leftarrow p_\Lambda + \eta \cdot \nabla_{p_\Lambda}(L_{PD})$ ▷ Adam update
  end procedure
end while

function ComputeResponsibilities(x)
  Compute the expected responsibilities for each mixture component
  Construct the responsibility vector C
  return C
end function

function NormalizedEntropy(C)
  Compute the entropy of responsibility vector C
  Normalize the entropy
  return Entropy_C
end function

4.1 Theoretical analysis

In this section, we extend S-IntroVAE by introducing a third player dedicated to modeling the prior. Our formulation draws inspiration from DeLiGAN Gurumurthy et al. (2017) where the noise in GANs was parametrized by a learnable MoG. In contrast to DeLiGAN, in our setting the prior (which is similar to the noise in GANs) has a dual role as (i) the source of the generated data distribution and (ii) the target

based on which the adversarial training is performed. We theoretically analyze the implication of training the prior within the S-IntroVAE and conclude that learning it in cooperation with the decoder constitutes a viable option for prior learning.

In our three-player setup the encoder q, the decoder d, and the prior λ are all flexible. We denote the generated data distribution as $p_d^\lambda(x) = \mathbb{E}_{p_\lambda(z)}[p_d(x \mid z)]$ to highlight its dependence on both the decoder d and the prior λ players. In that case, the adversarial game of equation 4 becomes:

$$\begin{aligned} L_q(\lambda, q, d) &= \mathbb{E}_{p_{\text{data}}}\left[W(x; \lambda, q, d)\right] - \mathbb{E}_{p_d^\lambda}\left[\frac{1}{\alpha} \cdot \exp(\alpha \cdot W(x; \lambda, q, d))\right], \\ L_d(\lambda, q, d) &= \mathbb{E}_{p_{\text{data}}}\left[W(x; \lambda, q, d)\right] + \gamma \cdot \mathbb{E}_{p_d^\lambda}\left[W(x; \lambda, q, d)\right]. \end{aligned} \tag{6}$$

The encoder is trained to maximize the L_q whereas the prior and the decoder maximize the L_d objective (i.e, prior–decoder cooperation). Below we show that prior–decoder cooperation is a viable option for prior learning which retains NE from the original S-IntroVAE formulation.

We modify equation 5 to support our learnable prior setup as: Let Λ denote the set of possible parameterizations of the prior and $\lambda \in \Lambda$.

Let us now define:

$$(\lambda^*, d^*) \in \arg\min_{\lambda, d} \left\{\text{KL}[p_{\text{data}}(x) || p_d^\lambda(x)] + \gamma \cdot \mathbb{H}[p_d^\lambda(x)]\right\}. \tag{7}$$

Let us also extend Assumption 1 to account for the prior being learnable.

Assumption 2. *For all x such that $p_{data}(x) \geq 0$ we have that $[p_{d^*}^{\lambda^*}(x)]^{\alpha+1} \leq p_{data}(x)$.*

Theorem 2. *Under the Assumption 2, when training the prior player λ in cooperation with the decoder player d then the triplet $q^* = p_{d^*}^{\lambda^*}(z|x)$, λ^* and d^* as defined in equation 7 constitutes a NE of the game equation 6.*

Our three-player formulation is similar in nature to S-IntroVAE with the encoder converging to the true posterior while the generated data distribution converges to an entropy-regularized version of the real data distribution. The key difference, however, lies in the fact that our formulation allows for a flexible prior, unlocking the merits of prior learning such as mitigating the prior hole problem, unsupervised clustering Dilokthanakul et al. (2016), explainability Klushyn et al. (2019), and more controllable generation Lavda et al. (2019). More specifically, for fixed encoder q and decoder d, given a batch of real and generated data respectively, the prior update seeks (i) to support a linear combination (controlled by the γ hyperparameter) of the empirical real and fake aggregated posterior and (ii) be idempotent under the projection by d.

4.1.1 Optimal ELBO in the Assumption-free setting

Theorem 2 requires Assumption 2 to hold, however, in practice this might not be the case, especially early in training. For instance, having a $p_d^\lambda(x)$ generating (i) out-of-distribution data or (ii) realistic samples at a disproportionately higher rate compared to the real distribution, are two obvious cases where such an assumption is violated. Analyzing the behavior of the encoder in these cases provides an intuitive connection to regularly trained VAEs and motivates some of our implementation choices. Let $\mathbb{X} = \{x | x \in p_{\text{data}}(x) > 0 \cup p_d^\lambda(x) > 0\}$ (i.e. the set of all possible samples in the union of real and generated data supports), we define the ELBO $W(x; \lambda, q^*, d)$ as:

$$W(x; \lambda, q^*, d) = \begin{cases} -\infty, \; x \in \{x \in \mathbb{X} \mid p_{\text{data}}(x) = 0\} \\ \frac{1}{\alpha} \cdot \log \frac{p_{\text{data}}(x)}{p_d^\lambda(x)}, \; x \in \{x \in \mathbb{X} \mid p_{\text{data}}(x) > 0 \cap [p_d^\lambda(x)]^{\alpha+1} > p_{\text{data}}(x)\} \\ \log p_d^\lambda(x), \; x \in \{x \in \mathbb{X} \mid p_{\text{data}}(x) > 0 \cap [p_d^\lambda(x)]^{\alpha+1} \leq p_{\text{data}}(x)\}\} \end{cases} \tag{8}$$

Proposition 1. *Given a fixed generated data distribution $p_d^\lambda(x)$ the q^* maximizing $L_q(\lambda, d, q)$ in Eq. 6 is such that the ELBO $W(x; \lambda, q^*, d)$ satisfies Eq. 43.*

The proposition above suggests that under the Assumption 2 the encoder in S-IntroVAE behaves similar to the one in regular VAEs. Alternatively, as a consequence of the repelling objective acting on the generated data, the encoder in S-IntroVAE diverges from its VAE-optimal state. This divergence depends on the sample-wise mismatch between $p_d^\lambda(x)$ and $p_{\text{data}}(x)$. Interestingly, it also appears that the optimal ELBO with respect to the encoder is a continuous function of the $p_{\text{data}}(x)$ measure. We refer to B.3 for practical implications of Proposition 1.

4.2 Implementation

In this section, we outline some implementation choices as well as the motivation behind them enabling prior learning in S-IntroVAE in a prior–decoder cooperation manner. Pseudo-code for the prior learning in S-IntroVAE is provided in Algorithm 1.

4.2.1 Prior as Source and Target

In the prior–decoder cooperation setting the prior player λ maximizes $L_d(\lambda, q, d)$. In practice, given a real x_{real} and $z_s \sim p_\lambda(z)$, the prior minimizes the loss $L_P(x_{\text{real}}, z_s)$ given by:

$$\begin{aligned} L_P(x_{\text{real}}, z_s) =& \beta_{\text{rec}} \cdot L_{\text{rec}}(x_{\text{real}}) + \beta_{\text{KL}} \cdot L_{\text{KL}}(x_{\text{real}}) + \gamma \cdot \big(\gamma_r \cdot \beta_{\text{rec}} \cdot L_{\text{rec}}(\texttt{sg}(D(z_s))) \\ &+ \beta_{\text{KL}} \cdot L_{\text{KL}}(D(z_s))\big), \end{aligned} \tag{9}$$

where $D(z_s)$ is the fake sample generated from decoding the latent z_s, while L_{rec} and L_{KL} the reconstruction and the KL losses respectively. We remained consistent with the S-IntroVAE, where the reconstruction of fake data was scaled by $\gamma_r = 10^{-8}$, and the stop-gradient ($\texttt{sg}$) operator was applied when generating a fake sample before computing its reconstruction loss. Additionally, we observe that the reconstruction loss for the real sample is not affected by the prior. In light of these, the prior player is trained both as a target for the real and fake posterior and as a source of fake samples. Based on that, a subtle issue arises when minimizing the $L_{\text{KL}}(D(z_s))$ term, since the prior can minimize it by either becoming a good source for generating realistic data or a good target that supports the posterior of generated data of low quality. The latter case is particularly problematic during the early stages of training, when the generated data lie outside the support of the real data, causing the encoder to assign a suboptimal posterior, as described in Proposition 1. To address this, we follow Shocher et al. (2023) and apply the $\texttt{sg}$ operator to the prior as the target while allowing gradient flow for the prior as the source when computing L_{KL} for the fake samples. We henceforth refer to this modified L_{KL} as $L_{\text{KL}}^{\texttt{sg}}$ which replaces the original when computing the KL loss of the $(D(z_s)$ in equation 9.

4.2.2 Adaptive Variance Soft-clipping

Although theoretically sound, the prior–decoder cooperation scheme led to instabilities manifested as exploding prior log-variances (see Fig. 2a) that became evident as the real data distribution became more complex (e.g. CIFAR-10 images vs 2D data). We attribute the aforementioned behavior to the interplay of three aspects: (i) the encoder pushing to suboptimal ELBOs (i.e. suboptimal reconstruction and KL losses) for those samples whose likelihood in fake data distribution is not sufficiently enclosed by the real one (see Proposition 1), (ii) hyperparameter-tuning caveats where good results generally required setting the β_{KL} of the fake ELBO (termed as β_{neg}) to be an order of magnitude of the latent dimension Daniel & Tamar (2021) and (iii) the behavior of the target distribution in KL minimization where the target variance increases when the source posterior and the target mean are far apart. Notably, (i) and (ii) promote the posterior of the real samples that overlap with insufficiently enclosed fake ones to diverge from the prior whereas (iii) increases the variance of the prior in an attempt to support a diverging aggregated posterior, which can lead to exploding log-variance in severe cases of (i). Eliminating (i) or (ii) requires extensive hyper-parameter tuning for each p_{data}, assuming that such a hyper-parameter set even exists. Instead, we opted to address the issue of exploding log-variances by tackling (iii). Namely, we employed an adapting soft-clipping scheme

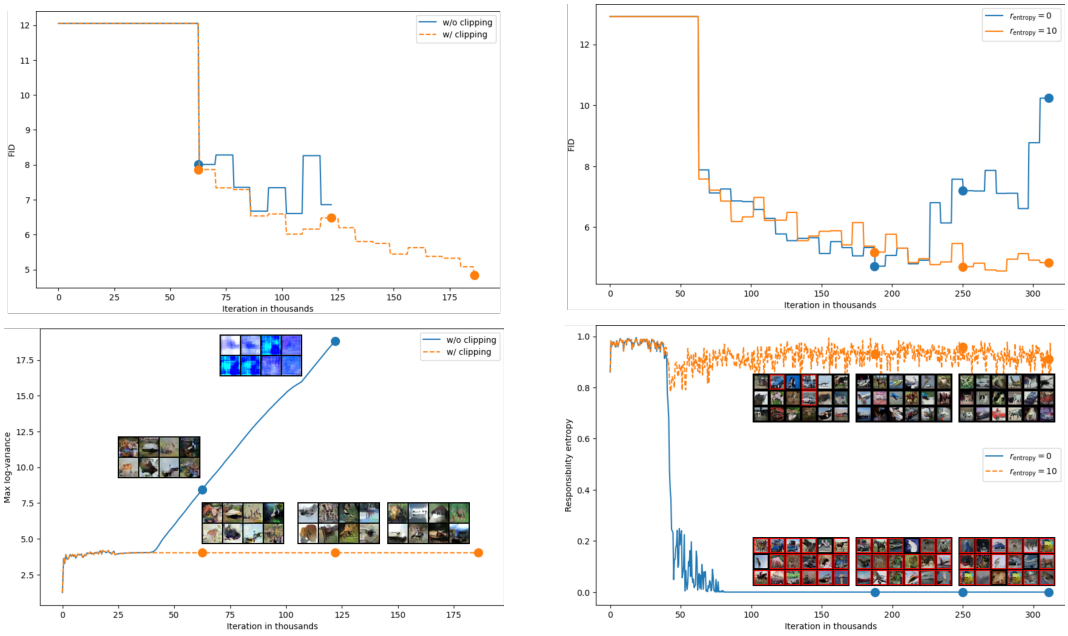

(a) (b)

Figure 2: Regularization for robust prior learning in S-IntroVAE. (a) Clipping the log-variance is crucial for maintaining the stability of S-IntroVAE under the prior–decoder cooperation. Two models were trained on CIFAR-10 for 120 epochs or until crashing. Without clipping, the log-variance tends to explode, leading to an increase in the FID metric and ultimately causing the model to generate indiscernible patterns before crashing. An unimodal MoG learnable prior was used for both models differing only by the log-variance clipping. (b) Emerging mode collapse due to unconstrained generation. We trained two models on CIFAR-10 for 200 epochs under a 10-modal MoG (log-variance clipped), differing only in the amount of entropy regularization. The red border indicates samples generated by inactive modes (i.e. average responsibility smaller than 10^{-2}). Note that not regularizing the responsibility entropy quickly degenerates into an unimodal prior setting where a single mode is responsible for supporting the aggregated posterior. The unimodal collapse eventually leads to mode collapse and an increase in FID due to the unconstrained generation originating from the inactive modes. On the contrary, regularizing the responsibility entropy maintains more uniform responsibility allocation among the modes and addresses the mode collapse issue.

inspired by Chua et al. (2018); Chang et al. (2023) where instabilities were also observed when learning log-variances. Concretely, the prior log-variance of the j^{th} latent dimension are clipped within the $[a_j, b_j]$ according to the clipping function f_c defined as:

$$f_c(x) = x + \frac{1}{\beta_j} \cdot \log \frac{1 + \exp(\beta_j \cdot (a_j - x))}{1 + \exp(\beta_j \cdot (x - b_j))}, \tag{10}$$

with $\beta_j = \frac{K}{b_j - a_j}$ and K a positive hyperparameter. The formulation above allows for controlling the steepness of clipping in a unified way using a single hyperparameter K for all latent dimensions. We elaborate further on this choice in C.1.

4.2.3 Responsibilities Regularization

Due to the nature of the L_q objective inducing the encoder to act as a discriminator between real and fake data, it is evident that the posterior can diverge arbitrarily from the prior (see Proposition 1).

In practice, we observed that such behavior can cause certain prior components to become more dominant than others in terms of the responsibilities of prior modes to posterior, leading to the formation of inactive

prior modes and vanishing gradients. Consequently, as the aggregated posterior is only supported by a portion of the prior modes, there are not multiple real samples competing for the same region of the latent space leading to unconstrainted generation when sampling for those inactive prior modes (see Fig. 2b). Note that the issue of inactive prior modes formation is applicable both when having a learnable (prior–decoder cooperation) and fixed MoG prior. To alleviate this we employ an entropy regularization on the responsibilities of each prior component discouraging inactive modes from forming. Concretely, the responsibility c_i corresponding to the i^{th} mode is computed as:

$$c_i = \mathbb{E}_{x\sim p_{\text{data}}(x)}\mathbb{E}_{z\sim q_\phi(z|x)}\left[\frac{w_i \cdot \mathcal{N}(z|\mu_i, \sigma_i^2 I)}{\sum_{l=1}^{M} w_l \cdot \mathcal{N}(z|\mu_l, \sigma_l^2 I)}\right]. \tag{11}$$

Finally, we define the responsibility vector $C = [c_1, c_2, \ldots, c_M]$ and compute its normalized entropy [1] $\mathbb{H}_n(C)$. The $\mathbb{H}_n(C)$ weighted by a non-negative hyperparameter r_{entropy}, is added to the L_q objective. Notably, our responsibility regularization is closely related to the mean entropy maximization regularizer used by Assran et al. (2022); Joulin & Bach (2012) regularizing the mode assignments instead of cluster assignments. Ultimately, encouraging uniform responsibilities accounts for the vanishing gradient issue as detailed in C.3, along with the derivation of the mode responsibility. Fig 2b illustrates a representative case of responsibility entropy development when left unregularized. Note that the responsibility regularization is relevant only for multi-modal priors and therefore not needed in the original S-IntroVAE under the standard Gaussian prior.

5 Experiments

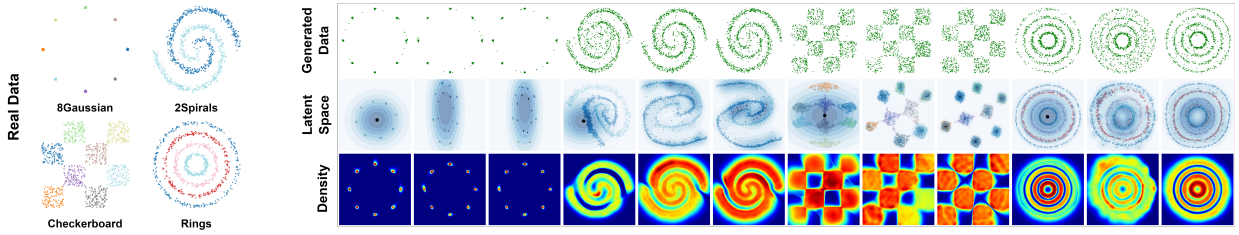

(a) (b)

Figure 3: (a) Real data (b) Qualitative results on density estimation, within each dataset we provide, from left to right, the results under the standard Gaussian, fixed and flexible MoG with learnable contributions corresponding to the 2^{nd}, 5^{th} and 6^{th} columns in Table 1 respectively.

5.1 2D - Density estimation

For the Density estimation benchmark, we adopt the same evaluation scheme as originally used in S-IntroVAE (Daniel & Tamar, 2021), namely, we use the gnELBO (grid-normalized ELBO) and the histogram-based KL and JSD (Jensen–Shannon divergence) divergences as measures of the inference, the forward and reverse generation capabilities, respectively.

To understand how modeling the prior as a third player affects S-IntroVAE we compare three discrete prior settings, namely (i) SG, (ii) fixed MoG and (iii) learnable MoG in decoder-cooperation, termed as Intro-Prior (IP) (see Fig. 1 for a conceptual visualization of the three settings). When utilizing MoG priors we experimented with both uniform and learnable contribution (LC) of each mode while we modeled the multi-modal prior using 64 components. More specifically, for the LC configuration, the contributions were learnable both for (ii) and (iii) during the VAE pre-training stage whereas during the adversarial training remained learnable only for (iii). The VampPrior was used during the VAE stage due to its benefits in latent space structuring over the MoG (Tomczak & Welling, 2018). The latter was turned into a MoG during the

[1] The entropy is normalized by dividing it by the maximum entropy given M possible assignments, where M is the number of prior components in the MoG.

adversarial training to ensure prior–decoder cooperation and to exploit the properties of its NE as given by Theorem 2. More specifically, we note that under the VampPrior, the prior is paired with the encoder establishing a prior–encoder cooperation. As analyzed in B.2.1, this cooperation leads to the prior and the decoder pulling the generated data distribution toward potentially incompatible objectives. When it comes to the regularizations, the beta-adapting log-variance clipping was used for IP with $K = 10$ and $[a_j, b_j]$ set to the minimum and maximum log-variance in each latent dimension j as found during the VAE warm-up while the mode responsibilities were left unregularized (i.e. $r_{\text{entropy}} = 0$). For all prior settings, we used 100 Monte Carlo samples to approximate the KL divergence between uni- and multi-modal Gaussian distributions.

In line with Daniel & Tamar (2021), we identified the optimal hyperparameters (i.e. β_{rec}, β_{KL} and β_{neg}) by performing an extensive grid-search while we used $\alpha = 2$ and $\gamma = 1$. In Table 1 we report the average (mean $\pm$ standard deviation) performance across five seeds. The quantitative results suggest that in most cases, IP improves the generation performance compared to when using the SG prior or the fixed MoG. In particular, this is more evident when looking at the histogram-based KL metric. The observation above aligns with our intuition as according to Theorem 2 both the prior and the decoder players cooperate towards minimizing the $\text{KL}[p_{\text{data}}(x)||p_d^{\lambda}(x)]$ term boosting the forward generation performance. When evaluating the qualitative performance as depicted in Fig. 3 we observe that the IP formulation tends to give rise to better-separated clusters in the latent space, more intuitive support of the aggregated posterior, and fewer samples in between the modes.

		VAE	S-IntroVAE				
		SG	SG	VAMP(64) → MoG(64)			
	LC	✗	✗	✗	✗	✓	✓
	IP	✗	✗	✗	✓	✗	✓
8Gaussian	gnELBO ↓	7.48 ±0.08	0.51 ±0.15	3.62 ±0.7	4.8 ±0.34	**0.25 ±0.04**	0.26 ±0.08
	KL ↓	6.94 ±0.81	**1.23 ±0.11**	4.46 ±5.89	2.36 ±0.67	1.94 ±0.75	2.24 ±1.6
	JSD ↓	17.41 ±0.28	**1.01 ±0.18**	1.77 ±1.56	1.79 ±0.2	1.13 ±0.28	1.08 ±0.15
2Spirals	gnELBO ↓	6.23 ±0.03	6.41 ±0.61	6.41 ±0.96	6.04 ±0.8	**5.81 ±0.9**	6.47 ±0.63
	KL ↓	10.18 ±0.36	9.5 ±1.23	8.61 ±0.79	8.31 ±0.45	9.45 ±1.25	**8.02 ±0.25**
	JSD ↓	4.94 ±0.24	4.21 ±0.5	3.76 ±0.09	**3.53 ±0.09**	3.89 ±0.18	3.64 ±0.16
Checkerboard	gnELBO ↓	8.62 ±0.11	**7.21 ±0.12**	8 ±0.07	7.66 ±0.29	7.81 ±0.21	7.67 ±0.12
	KL ↓	20.79 ±0.17	19.62 ±0.57	18.58 ±0.49	18.72 ±0.6	19.04 ±1.45	**17.7 ±0.25**
	JSD ↓	9.97 ±0.14	8.87 ±0.15	8.65 ±0.1	8.71 ±0.17	8.9 ±0.49	**8.46 ±0.15**
Rings	gnELBO ↓	6.37 ±0.09	**6.03 ±0.12**	6.73 ±0.4	6.86 ±0.35	6.4 ±0.75	6.65 ±0.41
	KL ↓	13.3 ±0.63	9.99 ±0.59	10.07 ±0.82	**9.77 ±0.7**	11.31 ±1.25	10.31 ±2.29
	JSD ↓	7.4 ±0.17	**4.05 ±0.15**	4.13 ±0.18	4.12 ±0.15	5.19 ±0.74	4.33 ± 0.73

Table 1: Quantitative performance on the four 2D datasets was evaluated.

5.2 Image Generation

We investigate whether and to which extent prior learning improves the generation performance and the representation learned using the (F)-MNIST and CIFAR-10 datasets. We evaluate the generation quality using the FID metric for samples generated from sampling from the prior and the aggregated posterior denoted as FID(GEN) and FID(REC) respectively.

The quality of the representations learned by the encoder was evaluated by fitting a linear SVM, similar to Kviman et al. (2023), using 2K-SVM and 10K-SVM iterations as well as utilizing a k-nearest neighbor classifier (k-NN) using 5-NN or 100-NN (Caron et al., 2021).

We use the default training hyperparameters and architectures as provided by Daniel & Tamar (2021) to train the S-IntroVAE, except that the first 20 epochs were used as a VAE training warm-up. We conduct experiments using the same configuration used for the 2D data, while we employ the r_{entropy} regularization with a value chosen from $\{0, 1, 10, 100\}$ and report the quantitative results for the one that led to the optimal FID(GEN) for each prior setting. The prior was modeled using 10 and 100 components and found that the latter is superior across all metrics, whether using the fixed or learnable MoG configurations, which is an indication that using a sufficiently large number of components is essential. The results provided in Tab. 5 suggest that replacing the SG with a MoG prior can benefit both the quality of the generation and the learned representation, however, the benefit is less profound in CIFAR-10 compared to the (F)-MNIST datasets. We attribute this behavior to CIFAR-10 potentially being (close-to) uni-modal distribution (Salmona et al., 2022) as opposed to (F)-MNIST which are more likely to be multi-modal. Furthermore, we observe that learning the prior during the adversarial training, as enabled by our IP formulation, generally outperformed training under a fixed MoG in MNIST and CIFAR10.

		S-IntroVAE				
		SG	VAMP(100) → MoG(100)			
	LC	✗	✗	✗	✓	✓
	IP	✗	✗	✓	✗	✓
MNIST	r_{entropy}	0	10	10	1	10
	Entr.	0	0.892 ±0.003	0.882 ±0.003	0.882 ±0.004	0.853 ±0.007
	FID (GEN) ↓	1.414 ±0.044	1.322 ±0.044	1.352 ±0.09	1.32 ±0.105	**1.309 ±0.046**
	FID (REC) ↓	1.503 ±0.053	**1.342 ±0.087**	1.473 ±0.174	1.363 ±0.13	1.385 ±0.141
	2K-SVM ↑	0.93 ±0.002	0.961 ±0.002	0.97 ±0.007	0.962 ±0.003	**0.972 ±0.003**
	10K-SVM ↑	0.93 ±0.002	0.961 ±0.002	0.97 ±0.007	0.962 ±0.003	**0.972 ±0.003**
	5-NN ↑	0.763 ±0.005	0.916 ±0.007	0.947 ±0.019	0.92 ±0.002	**0.957 ±0.007**
	100-NN ↑	0.87 ±0.006	0.934 ±0.004	0.953 ±0.013	0.935 ±0.002	**0.958 ±0.004**
FMNIST	r_{entropy}	0	0	10	10	10
	Entr.	0	0.931 ±0.005	0.931 ±0.002	0.944 ±0.001	0.903 ±0.009
	FID (GEN) ↓	3.326 ±0.067	2.785 ±0.088	3.025 ±0.241	**2.727 ±0.137**	2.831 ±0.173
	FID (REC) ↓	3.76 ±0.168	**2.994** ±0.087	3.129 ±0.165	3.185 ±0.175	3.511 ±0.128
	2K-SVM ↑	0.681 ±0.002	**0.731 ±0.005**	0.695 ±0.011	0.712 ±0.009	0.696 ±0.004
	10K-SVM ↑	0.731 ±0.011	**0.78 ±0.003**	0.772 ±0.005	0.778 ±0.003	0.773 ±0.004
	5-NN ↑	0.425 ±0.016	0.683 ±0.011	0.693 ±0.014	0.678 ±0.01	**0.707 ±0.009**
	100-NN ↑	0.606 ±0.024	0.736 ±0.006	0.729 ±0.01	0.731 ±0.006	**0.739 ±0.007**
CIFAR-10	r_{entropy}	0	10	100	100	10
	Entr.	0	0.839 ±0.012	0.94 ±0.004	0.929 ±0.006	0.511 ±0.074
	FID (GEN) ↓	4.424 ±0.11	4.465 ±0.066	**4.385 ±0.242**	4.417 ±0.054	4.594 ±0.407
	FID (REC) ↓	4.13 ±0.119	4.205 ±0.157	**4.084 ±0.011**	4.141 ±0.068	4.585 ±0.645
	2K-SVM ↑	0.245 ±0.015	0.25 ±0.003	**0.271 ±0.011**	0.26 ±0.003	0.256 ±0.005
	10K-SVM ↑	0.391±0.009	0.396 ±0.004	**0.407 ±0.013**	0.401 ±0.003	0.396 ±0.003
	5-NN ↑	0.206 ±0.002	0.189 ±0	**0.239 ±0.009**	0.196 ±0.002	0.219 ±0.004
	100-NN ↑	0.308 ±0.012	0.216 ±0.015	**0.32 ±0.009**	0.259 ±0.005	0.273 ±0.008

Table 2: Quantitative performance on the images datasets. The r_{entropy} row corresponds to the regularization used to obtain the optimal FID(GEN) for each training configuration, where the Entr. row refers to the normalized entropy of the responsibilities where the closer to one its value the more uniformly the aggregated posterior is supported by the prior components.

Interestingly, learning the prior improves classification performance under the k-NN model across all datasets. This suggests that prior learning in S-IntroVAE leads to a more defined class separation and more interpretable latent space, where similar samples are more effectively clustered together.

A qualitative inspection of the latent space (see Fig. 4) reveals that modeling the prior as a mixture of MoG results in better-separated clusters compared to a standard Gaussian. When comparing a fixed MoG (w/o IP) to a learnable MoG (w/ IP), the improvement in class separation is less pronounced but still noticeable. For the complete results and latent space visualization, we refer the readers to D.2 and D.4.

Finally, it is worth noting how the entropy regularization behaves differently based on the training hyperparameters, dataset complexity and prior learning configuration. In this regard, we observe that a higher r_{entropy} was necessary to achieve the optimal performance on CIFAR-10 compared to the (F)-MNIST datasets under the IP configuration. Additionally, allowing for learnable contributions under the IP configuration tends to decrease the normalized entropy of the responsibilities suggesting that contributions tend to vanish as soon as they no longer support the aggregated posterior which advocates for the importance of taking measures (e.g. using the r_{entropy}) to utilize all the components when performing the discrimination (i.e. updating the encoder).

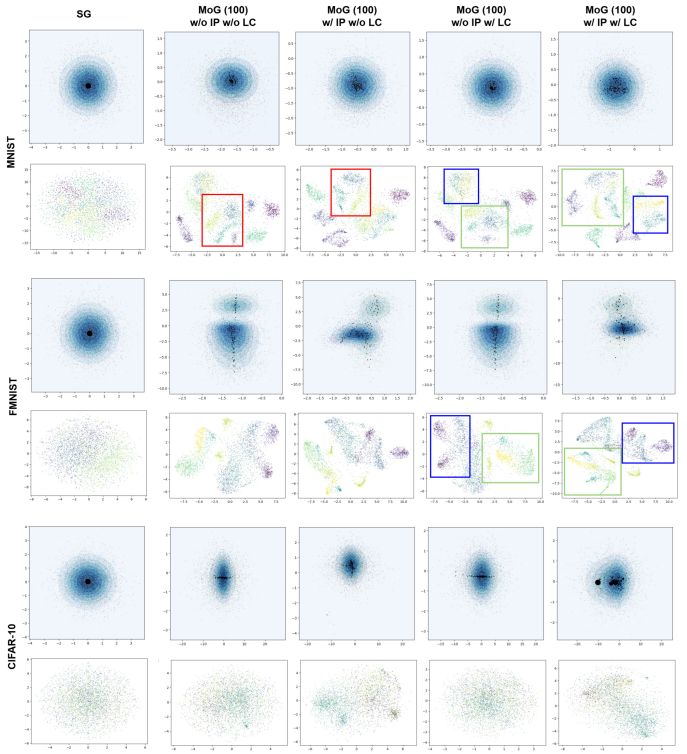

Figure 4: Visualizing the first two latent dimensions of the latent space and the t-SNE 2D embeddings of the full latent space. The columns correspond to those in Tab. 5. Different colors correspond to different classes. The black dots refer to the means of the prior components and their size corresponds to their contribution weight.

6 Conclusions

In this study, we have proposed a prior-decoder cooperation scheme as a theoretically sound approach to prior learning in S-IntroVAE, marking the first successful integration of prior learning in Introspective VAEs. Our approach aims to combine two independent directions for improving VAEs: prior learning and the incorporation of adversarial objectives. To realize our proposed scheme, we identified several challenges, which we addressed with theoretically motivated regularization techniques, specifically (i) adaptive log-variance clipping and (ii) responsibility regularization. Our experimental results conducted in 2D and high-dimensional image settings demonstrate the benefits of learning the prior in S-IntroVAE. These benefits include a better-structured and more explainable latent space and, in most cases, improved generation performance. We firmly believe that our theoretical insights, coupled with the empirical results, pave the way towards a better understanding of Introspective VAEs and their connection to their VAEs and GANs counterparts. Finally, owing to the unique nature of the problem where a multimodal distribution constitutes both the source and the target, we hope that our analyses enjoy practical use in other areas that deal with problems of similar characteristics e.g. Idempotent Generative Networks (Shocher et al., 2023) or adversarially robust clustering (Yang et al., 2020).

References

Jyoti Aneja, Alex Schwing, Jan Kautz, and Arash Vahdat. A contrastive learning approach for training variational autoencoder priors. Advances in neural information processing systems, 34:480–493, 2021.

Mahmoud Assran, Mathilde Caron, Ishan Misra, Piotr Bojanowski, Florian Bordes, Pascal Vincent, Armand Joulin, Mike Rabbat, and Nicolas Ballas. Masked siamese networks for label-efficient learning. In European Conference on Computer Vision, pp. 456–473. Springer, 2022.

Yuri Burda, Roger Grosse, and Ruslan Salakhutdinov. Importance weighted autoencoders. arXiv preprint arXiv:1509.00519, 2015.

Mathilde Caron, Hugo Touvron, Ishan Misra, Hervé Jégou, Julien Mairal, Piotr Bojanowski, and Armand Joulin. Emerging properties in self-supervised vision transformers. In Proceedings of the IEEE/CVF international conference on computer vision, pp. 9650–9660, 2021.

Bo Chang, Alexandros Karatzoglou, Yuyan Wang, Can Xu, Ed H Chi, and Minmin Chen. Latent user intent modeling for sequential recommenders. In Companion Proceedings of the ACM Web Conference 2023, pp. 427–431, 2023.

Kushal Chauhan, Pradeep Shenoy, Manish Gupta, Devarajan Sridharan, et al. Robust outlier detection by de-biasing vae likelihoods. In Proceedings of the IEEE/CVF Conference on Computer Vision and Pattern Recognition, pp. 9881–9890, 2022.

Rewon Child. Very deep vaes generalize autoregressive models and can outperform them on images. arXiv preprint arXiv:2011.10650, 2020.

Kurtland Chua, Roberto Calandra, Rowan McAllister, and Sergey Levine. Deep reinforcement learning in a handful of trials using probabilistic dynamics models. Advances in neural information processing systems, 31, 2018.

Marissa Connor, Gregory Canal, and Christopher Rozell. Variational autoencoder with learned latent structure. In International Conference on Artificial Intelligence and Statistics, pp. 2359–2367. PMLR, 2021.

Tal Daniel and Aviv Tamar. Soft-introvae: Analyzing and improving the introspective variational autoencoder. In Proceedings of the IEEE/CVF Conference on Computer Vision and Pattern Recognition, pp. 4391–4400, 2021.

Nat Dilokthanakul, Pedro AM Mediano, Marta Garnelo, Matthew CH Lee, Hugh Salimbeni, Kai Arulkumaran, and Murray Shanahan. Deep unsupervised clustering with gaussian mixture variational autoencoders. arXiv preprint arXiv:1611.02648, 2016.

Ioannis Gatopoulos and Jakub M Tomczak. Self-supervised variational auto-encoders. Entropy, 23(6):747, 2021.

Ian Goodfellow, Jean Pouget-Abadie, Mehdi Mirza, Bing Xu, David Warde-Farley, Sherjil Ozair, Aaron Courville, and Yoshua Bengio. Generative adversarial networks. Communications of the ACM, 63(11): 139–144, 2020.

Prasoon Goyal, Zhiting Hu, Xiaodan Liang, Chenyu Wang, and Eric P Xing. Nonparametric variational auto-encoders for hierarchical representation learning. In Proceedings of the IEEE International Conference on Computer Vision, pp. 5094–5102, 2017.

Swaminathan Gurumurthy, Ravi Kiran Sarvadevabhatla, and R Venkatesh Babu. Deligan: Generative adversarial networks for diverse and limited data. In Proceedings of the IEEE conference on computer vision and pattern recognition, pp. 166–174, 2017.

Irina Higgins, Loic Matthey, Arka Pal, Christopher Burgess, Xavier Glorot, Matthew Botvinick, Shakir Mohamed, and Alexander Lerchner. beta-vae: Learning basic visual concepts with a constrained variational framework. 2016.

Jonathan Ho, Ajay Jain, and Pieter Abbeel. Denoising diffusion probabilistic models. Advances in neural information processing systems, 33:6840–6851, 2020.

Matthew D Hoffman and Matthew J Johnson. Elbo surgery: yet another way to carve up the variational evidence lower bound. In Workshop in Advances in Approximate Bayesian Inference, NIPS, volume 1, 2016.

Huaibo Huang, Ran He, Zhenan Sun, Tieniu Tan, et al. Introvae: Introspective variational autoencoders for photographic image synthesis. Advances in neural information processing systems, 31, 2018.

Xu Ji, Lena Nehale-Ezzine, and Maksym Korablyov. Properties of minimizing entropy. arXiv preprint arXiv:2112.03143, 2021.

Armand Joulin and Francis Bach. A convex relaxation for weakly supervised classifiers. arXiv preprint arXiv:1206.6413, 2012.

Dimitris Kalatzis, David Eklund, Georgios Arvanitidis, and Søren Hauberg. Variational autoencoders with riemannian brownian motion priors. arXiv preprint arXiv:2002.05227, 2020.

Diederik P Kingma and Max Welling. Auto-encoding variational bayes. arXiv preprint arXiv:1312.6114, 2013.

Alexej Klushyn, Nutan Chen, Richard Kurle, Botond Cseke, and Patrick van der Smagt. Learning hierarchical priors in vaes. Advances in neural information processing systems, 32, 2019.

Oskar Kviman, Ricky Molén, Alexandra Hotti, Semih Kurt, Vıctor Elvira, and Jens Lagergren. Cooperation in the latent space: The benefits of adding mixture components in variational autoencoders. In International Conference on Machine Learning, pp. 18008–18022. PMLR, 2023.

Anders Boesen Lindbo Larsen, Søren Kaae Sønderby, Hugo Larochelle, and Ole Winther. Autoencoding beyond pixels using a learned similarity metric. In International conference on machine learning, pp. 1558–1566. PMLR, 2016.

Frantzeska Lavda, Magda Gregorová, and Alexandros Kalousis. Improving vae generations of multimodal data through data-dependent conditional priors. arXiv preprint arXiv:1911.10885, 2019.

Shuyu Lin and Ronald Clark. Ladder: Latent data distribution modelling with a generative prior. arXiv preprint arXiv:2009.00088, 2020.

Alireza Makhzani, Jonathon Shlens, Navdeep Jaitly, and Ian Goodfellow. Adversarial autoencoders. In International Conference on Learning Representations, 2016. URL http://arxiv.org/abs/1511.05644.

Lars Mescheder, Andreas Geiger, and Sebastian Nowozin. Which training methods for gans do actually converge? In International conference on machine learning, pp. 3481–3490. PMLR, 2018.

Konpat Preechakul, Nattanat Chatthee, Suttisak Wizadwongsa, and Supasorn Suwajanakorn. Diffusion autoencoders: Toward a meaningful and decodable representation. In Proceedings of the IEEE/CVF Conference on Computer Vision and Pattern Recognition, pp. 10619–10629, 2022.

Ali Razavi, Aaron Van den Oord, and Oriol Vinyals. Generating diverse high-fidelity images with vq-vae-2. Advances in neural information processing systems, 32, 2019.

Luis A Pérez Rey, Vlado Menkovski, and Jacobus W Portegies. Diffusion variational autoencoders. arXiv preprint arXiv:1901.08991, 2019.

Danilo Jimenez Rezende and Fabio Viola. Taming vaes. arXiv preprint arXiv:1810.00597, 2018.

Danilo Jimenez Rezende, Shakir Mohamed, and Daan Wierstra. Stochastic backpropagation and approximate inference in deep generative models. In International conference on machine learning, pp. 1278–1286. PMLR, 2014.

Antoine Salmona, Valentin De Bortoli, Julie Delon, and Agnès Desolneux. Can push-forward generative models fit multimodal distributions? Advances in Neural Information Processing Systems, 35:10766–10779, 2022.

Assaf Shocher, Amil Dravid, Yossi Gandelsman, Inbar Mosseri, Michael Rubinstein, and Alexei A Efros. Idempotent generative network. arXiv preprint arXiv:2311.01462, 2023.

Casper Kaae Sønderby, Tapani Raiko, Lars Maaløe, Søren Kaae Sønderby, and Ole Winther. Ladder variational autoencoders. Advances in neural information processing systems, 29, 2016.

Jakub Tomczak and Max Welling. Vae with a vampprior. In International Conference on Artificial Intelligence and Statistics, pp. 1214–1223. PMLR, 2018.

Jakub M Tomczak. Deep generative modeling. Springer, 2022.

Arash Vahdat and Jan Kautz. Nvae: A deep hierarchical variational autoencoder. Advances in Neural Information Processing Systems, 33:19667–19679, 2020.

Ling Yang, Zhilong Zhang, Yang Song, Shenda Hong, Runsheng Xu, Yue Zhao, Yingxia Shao, Wentao Zhang, Bin Cui, and Ming-Hsuan Yang. Diffusion models: A comprehensive survey of methods and applications. arXiv preprint arXiv:2209.00796, 2022.

Xu Yang, Cheng Deng, Kun Wei, Junchi Yan, and Wei Liu. Adversarial learning for robust deep clustering. Advances in Neural Information Processing Systems, 33:9098–9108, 2020.

Zilong Yu, Yunyun Yang, Yongbin Zhu, Bixue Guo, and Chun Li. Cs-introvae: Cauchy-schwarz divergence-based introspective variational autoencoder. IEEE Transactions on Multimedia, 2023.

Shengjia Zhao, Jiaming Song, and Stefano Ermon. Learning hierarchical features from deep generative models. In International Conference on Machine Learning, pp. 4091–4099. PMLR, 2017.

A Preliminaries

The ELBO, given a sample x, can be formulated as:

$$\begin{aligned} W(x;q,d) &= \mathbb{E}_{z\sim q_{(z|x)}}[\log p_d(x|z)] - \mathrm{KL}[q(z|x)||p(z)] \\ &= \mathbb{E}_{z\sim q_{(z|x)}}[\log p_d(x|z)] - \mathbb{E}_{z\sim q_{(z|x)}}[\log \frac{q(z|x)}{p_z(z)}] \\ &= \mathbb{E}_{z\sim q_{(z|x)}}[\log \frac{p_d(z|x)\cdot p_d(x)}{p_z(z)} - \log \frac{q(z|x)}{p_z(z)}] \\ &= \mathbb{E}_{z\sim q_{(z|x)}}[\log p_d(z|x) + \log p_d(x) - \log q(z|x)] \\ &= \log p_d(x) - \mathrm{KL}[q(z|x)||p_d(z|x)] \leq \log p_d(x), \end{aligned} \tag{12}$$

with $\mathrm{KL}[\cdot||\cdot]$ denoting the Kullback–Leibler (KL) divergence.

B Nash Equilibrium in S-IntroVAE

In this section, we provide the theorems based on which the prior–decoder cooperation emerges as a viable option for learning the prior in S-IntroVAE. First, we revisit the derivation of the Nash Equilibrium (NE), under the fixed prior case (originally provided by Daniel & Tamar (2021)), which we modify to account for samples outside the support of the real data distribution. The details and the motivation behind the aforementioned modification are provided in Section B.1.

For simplicity, our analysis is conducted in the discrete domain which is in practice sufficiently revealing as we deal with finite data. From a theoretical standpoint, we can rely on continuity arguments under the assumption of Leibniz's continuity.

B.1 S-IntroVAE under a fixed prior (Daniel & Tamar (2021))

The adversarial game as defined by Daniel & Tamar (2021):

$$\begin{aligned} L_q(q,d) &= \mathbb{E}_{p_{\text{data}}}\left[W(x;q,d)\right] - \mathbb{E}_{p_d}\left[\frac{1}{\alpha}\cdot\exp(\alpha\cdot W(x;q,d))\right], \\ L_d(q,d) &= \mathbb{E}_{p_{\text{data}}}\left[W(x;q,d)\right] + \gamma\cdot\mathbb{E}_{p_d}\left[W(x;q,d)\right], \end{aligned} \tag{13}$$

where $\alpha \geq 1$, $\gamma \geq 0$ and $p_d(x) = \mathbb{E}_{p(z)}[p_d(x|z)]$ with $p(z)$ a fixed prior distribution. Note that although originally, a standard Gaussian (SG) prior was used the derivation extends to any prior distribution as long as it is fixed. For notational brevity, we will henceforth refer to the expectation over the real data distribution $\mathbb{E}_{x\sim p_{\text{data}}}[\cdot]$ simply as $\mathbb{E}_{p_{\text{data}}}[\cdot]$, the same applies to the generated data distribution as well.

Lemma 1. *Assuming that $[p_d(x)]^{\alpha+1} \leq p_{data}(x)$ for all x such that $p_{data}(x) \geq 0$, the q^* maximizing the $L_q(q,d)$ satisfies $q^*(d)(z|x) = p_d(z|x)$.*

Remark 2. *The assumption used in Lemma 1 is a modified version of the one used in (Daniel & Tamar, 2021) in order to account for samples outside of the support of the $p_{data}(x)$. Specifically we require the assumption $[p_d(x)]^{\alpha+1} \leq p_{data}(x)$ to hold for all x such that $p_{data}(x) \geq 0$ instead to $p_{data}(x) > 0$. The utility of this modification is revealed in the proof below.*

Proof. Using the ELBO reformulation provided in 12 we develop the $L_q(q,d)$ objective as:

$$\begin{aligned} L_q(q,d) &= \mathbb{E}_{p_{\text{data}}}\left[W(x;q,d)\right] - \mathbb{E}_{p_d}\left[\frac{1}{\alpha}\cdot\exp(\alpha\cdot W(x;q,d))\right] \\ &= \mathbb{E}_{p_{\text{data}}}\left[\log p_d(x) - \text{KL}[q(z|x)||p_d(z|x)]\right] \\ &- \frac{1}{a}\cdot\mathbb{E}_{p_d}\left[\exp(\log[p_d(x)]^{\alpha} - \alpha\cdot\text{KL}[q(z|x)||p_d(z|x)])\right] \\ &= \mathbb{E}_{p_{\text{data}}}\left[\log p_d(x) - \text{KL}[q(z|x)||p_d(z|x)]\right] \\ &- \frac{1}{a}\cdot\mathbb{E}_{p_d}\left[[p_d(x)]^{\alpha}\cdot\exp(-\alpha\cdot\text{KL}[q(z|x)||p_d(z|x)])\right] \\ &= \sum_x p_{\text{data}}(x)\cdot(\log p_d(x) - \text{KL}[q(z|x)||p_d(z|x)]) - \frac{1}{\alpha}\cdot[p_d(x)]^{\alpha+1}\cdot\exp(-\alpha\cdot\text{KL}[q(z|x)||p_d(z|x)]) \\ &= \begin{cases} \sum_x p_{\text{data}}(x)\cdot\left(\log p_d(x) - \text{KL}[q(z|x)||p_d(z|x)] - \frac{1}{\alpha}\cdot\frac{[p_d(x)]^{\alpha+1}}{p_{\text{data}}(x)}\cdot\exp(-\alpha\cdot\text{KL}[q(z|x)||p_d(z|x)])\right) \\ = \sum_x G(q,d), \quad x\in\{p_{\text{data}}(x)>0\} \\ \\ \sum_x\left(-\frac{1}{\alpha}\cdot[p_d(x)]^{\alpha+1}\cdot\exp(-\alpha\cdot\text{KL}[q(z|x)||p_d(z|x)])\right) \\ = \sum_x Q(q,d), \quad x\in\{p_{\text{data}}(x)=0\} \end{cases} \end{aligned} \tag{14}$$

The optimal q^* for each x can be found as the maximizer of the $L_q(q,d)$.

Given x such that $p_{\text{data}}(x) > 0$ the optimal q^* can be found as the maximizer of the function $G(q,d)$. In that case, we observe that q contributes to $G(q,d)$ only via the KL term. Based on that, the saddle point can be found by analyzing the derivative of $G(q,d)$ with respect to the KL.

$$\frac{\partial G(q,d)}{\partial\text{KL}[q(z|x)||p_d(z|x)]} = p_{\text{data}}(x)\cdot\left(-1 + \frac{[p_d(x)]^{a+1}}{p_{\text{data}}(x)}\cdot\exp(-\alpha\cdot\text{KL}[q(z|x)||p_d(z|x)])\right). \tag{15}$$

For x such that $p_{\text{data}}(x) > 0$ and $\frac{[p_d(x)]^{\alpha+1}}{p_{\text{data}}(x)} < 1$, we observe that the $\frac{\partial G(q,d)}{\partial \text{KL}[q(z|x)||p_d(z|x)]} < 0$ for $\text{KL}(q(z|x)||p_d(z|x)) \in [0, \infty)$ (KL is non negative), that is the $G(q, d)$ monotonically decreases with respect to $\text{KL}[q(z|x)||p_d(z|x)]$.

For x such that $p_{\text{data}}(x) > 0$ and $\frac{[p_d(x)]^{\alpha+1}}{p_{\text{data}}(x)} = 1$ we observe that the $\frac{\partial G(q,d)}{\partial \text{KL}[q(z|x)||p_d(z|x)]} = 0$ only when $\text{KL}[q(z|x)||p_d(z|x)] = 0$.
Additionally $\frac{\partial G(q,d)}{\partial^2 \text{KL}[q(z|x)||p_d(z|x)]} = p_{\text{data}}(x) \cdot \left(-\alpha \cdot \frac{[p_d(x)]^{\alpha+1}}{p_{\text{data}}(x)} \cdot \exp(-\alpha \cdot \text{KL}[q(z|x)||p_d(z|x)])\right) \leq 0.$

Based on these two cases above, we conclude that $\text{KL}[q^*(z|x)||p_d(z|x)] = 0$ is a global maxima of $L_q(q, d)$ for x such that $p_{\text{data}}(x) > 0$ and $\frac{[p_d(x)]^{\alpha+1}}{p_{\text{data}}(x)} \leq 1$.

For x such that $p_{\text{data}}(x) = 0$ the optimal q^* can be found as the maximizer of the function $Q(q, d)$.

$$\frac{\partial Q(q, d)}{\partial \text{KL}[q(z|x)||p_d(z|x)]} = [p_d(x)]^{\alpha+1} \cdot \exp(-\alpha \cdot \text{KL}[q(z|x)||p_d(z|x)]). \tag{16}$$

We observe that $\frac{\partial Q(q,d)}{\partial \text{KL}[q(z|x)||p_d(z|x)]} > 0$, given that $\text{KL}[q(z|x)||p_d(z|x)] \in [0, \infty)$ we conclude $q^*(z|x)$ such that $\text{KL}[q^*(z|x)||p_d(z|x)] = \infty$ is a global maxima of $L_q(q, d)$ for x such that $p_{\text{data}}(x) = 0$. The result above contradicts what has been argued in (Daniel & Tamar, 2021) and is the motivation behind extending the assumption used in Lemma 1 to account for samples outside of the support of $p_{\text{data}}(x)$ (i.e. $p_{\text{data}}(x) \geq 0$ instead of $p_{\text{data}}(x) > 0$ used in (Daniel & Tamar, 2021)). Under the modified assumption, for x such that $p_{\text{data}}(x) = 0$ we also have $p_d(x) = 0$. In this case samples outside the support of the real data distribution do not contribute to the $L_q(q, d)$ objective and therefore do not influence the optimal q^*.

Given that the KL is a proper divergence and under the assumption that $[p_d(x)]^{\alpha+1} \leq p_{\text{data}}(x)$ holds for all x such that $p_{\text{data}}(x) \geq 0$, we conclude that $q^*(z|x) = p_d(z|x))$ is the global maxima of the $L_q(q, d)$, that is:

$$L_q(q(d), d) \leq L_q(q^*(d), d) \text{ for all } q. \tag{17}$$

□

Let us define d^* as:

$$d^* \in \arg\min_d \{\text{KL}[p_{data}(x)||p_d(x)] + \gamma \cdot \mathbb{H}[p_d(x)]\}. \tag{18}$$

Assumption 3 (Modified - (Daniel & Tamar, 2021))**.** *For all x such that $p_{data}(x) \geq 0$ we have that $[p_{d^*}(x)]^{\alpha+1} \leq p_{data}(x)$.*

Theorem 3 ((Daniel & Tamar, 2021))**.** *Under the Assumption 3, the pair of optimal $q^* = p_{d^*}(z|x)$ and d^* as defined in equation 18 constitutes a NE of the game equation 13.*

Proof. First, we develop the $L_d(q, d)$ as:

$$
\begin{aligned}
L_d(q,d) &= \mathbb{E}_{p_{\text{data}}}\left[W(x;q,d)\right] + \gamma \cdot \mathbb{E}_{p_d}\left[W(x;q,d)\right] \\
&= \mathbb{E}_{p_{\text{data}}}\left[\log p_d(x) - \mathrm{KL}[q(z|x)||p_d(z|x)]\right] \\
&+ \gamma \cdot \mathbb{E}_{p_d}\left[\log p_d(x) - \mathrm{KL}[q(z|x)||p_d(z|x)]\right] \\
&= \mathbb{E}_{p_{\text{data}}}\left[\log \frac{p_d(x)}{p_{\text{data}}(x)} + \log p_{\text{data}}(x) - \mathrm{KL}[q(z|x)||p_d(z|x)]\right] \\
&+ \gamma \cdot \mathbb{E}_{p_d}\left[\log p_d(x) - \mathrm{KL}[q(z|x)||p_d(z|x)]\right] \\
&= \mathbb{E}_{p_{\text{data}}}[\log p_{\text{data}}(x)] \\
&- \mathrm{KL}[p_{\text{data}}(x)||p_d(x)] - \gamma \cdot \mathbb{H}[p_d(x)] \\
&- \mathbb{E}_{p_{\text{data}}}[\mathrm{KL}[q(z|x)||p_d(z|x)]] - \gamma \cdot \mathbb{E}_{p_d}[\mathrm{KL}[q(z|x)||p_d(z|x)]],
\end{aligned}
\tag{19}
$$

with $\mathbb{H}[\cdot]$ denoting the Shannon entropy. Note that since $\mathrm{KL}[q(z|x)||p_d(z|x)] \geq 0 = \mathrm{KL}[q^*(z|x)||p_d(z|x)]$ the d^* maximizing the $L_d(q,d)$ can be found as the maximizer of $L_d(q^*,d)$. Based on that we set $q = q^*(d)$ in 19 and find the expression of d that maximizes the objective $L_d(q^*(d),d)$ as:

$$
\begin{aligned}
L_d(q^*(d),d) &= \mathbb{E}_{p_{\text{data}}}[\log p_{\text{data}}(x)] \\
&- \mathrm{KL}[p_{\text{data}}(x)||p_d(x)] - \gamma \cdot \mathbb{H}[p_d(x)] \\
&- \mathbb{E}_{p_{\text{data}}}[\mathrm{KL}[q^*(z|x)||p_d(z|x)]] - \gamma \cdot \mathbb{E}_{p_d}[\mathrm{KL}[q^*(z|x)||p_d(z|x)]],
\end{aligned}
\tag{20}
$$

where the two terms $\mathrm{KL}[q^*(z|x)||p_d(z|x)]$ are annotated with arrows to 0.

as the $\mathbb{E}_{p_{\text{data}}}[\log p_{\text{data}}(x)]$ is fixed given a distribution $p_{\text{data}(x)}$ while the $\mathrm{KL}[\cdot||\cdot]$ and $\mathbb{H}[\cdot]$ are non-negative, we can derive the maximizer d^* according to equation 18. Based on that and according to Lemma 1,

$$
\begin{aligned}
L_q(q(d^*),d^*) \leq L_q(q^*(d^*),d^*) \;\text{ for all }\; q, \\
L_d(q^*(d),d) \leq L_q(q^*(d^*),d^*) \;\text{ for all }\; d,
\end{aligned}
\tag{21}
$$

and therefore we conclude that the pair q^* and d^* such that:

$$
\begin{aligned}
q^*(z|x) &= p_{d^*}(z|x), \\
d^* &\in \arg\min_d \left\{\mathrm{KL}[p_{\text{data}}(x)||p_d(x)] + \gamma \cdot \mathbb{H}[p_d(x)]\right\}.
\end{aligned}
\tag{22}
$$

is a NE of the equation 13. □

We refer the readers to the original work by Daniel & Tamar (2021) for the proof that for any $p_{\text{data}}(x)$ there always exists $\gamma > 0$ such that the assumption 3 holds for $p_{d^*}(x)$.

B.2 S-IntroVAE under a learnable prior

Let Λ denote the set of possible parameterizations of the prior distributions. We now assume that the prior $p_z(z)$ is learnable and henceforth is denoted as $p_\lambda(z)$ with $\lambda \in \Lambda$ while the generated distribution under that prior is $p_d^\lambda(x) = \mathbb{E}_{p_\lambda(z)} p_d(x|z)$. Consequently the adversarial game equation 13 is modified as:

$$
\begin{aligned}
L_q(\lambda,q,d) &= \mathbb{E}_{p_{\text{data}}}\left[W(x;\lambda,q,d)\right] - \mathbb{E}_{p_d^\lambda}\left[\frac{1}{\alpha} \cdot \exp(\alpha \cdot W(x;\lambda,q,d))\right], \\
L_d(\lambda,q,d) &= \mathbb{E}_{p_{\text{data}}}\left[W(x;\lambda,q,d)\right] + \gamma \cdot \mathbb{E}_{p_d^\lambda}\left[W(x;\lambda,q,d)\right].
\end{aligned}
\tag{23}
$$

B.2.1 Prior–encoder Cooperation

Here we conjecture the infeasibility of learning the prior in collaboration with the encoder while maintaining the same NE of the S-IntroVAE. Intuitively, this formulation seeks to find the optimal prior as the balance between maximizing the real ELBO and minimizing the fake exp(ELBO).

Similarly, the definition in Eq equation 18 is modified as:

$$d^*(\lambda) \in \arg\min_d \left\{ \mathrm{KL}[p_{\mathrm{data}}(x)||p_d^\lambda(x)] + \gamma \cdot \mathbb{H}[p_d^\lambda(x)] \right\}, \tag{24}$$

to account for the parameterized prior. Let $p_d^\lambda(x)$ a discrete distribution of sample size N and e's non-negative real numbers realizing the unnormalized probability masses of $p_d^\lambda(x)$ distribution such that the likelihood of sample x_k is calculated as:

$$p_d^\lambda(x_k) = \frac{e_k}{\sum_{j=1}^{N} e_j}. \tag{25}$$

Let us define the entropy $\mathbb{H}[p_d^\lambda(x)]$ and the α-order regularization[2] $\mathbb{A}[p_d^\lambda(x)]$ as:

$$\mathbb{H}[p_d^\lambda(x)] = -\sum_{i=1}^{N} p_d^\lambda(x_i) \cdot \log\left(p_d^\lambda(x_i)\right), \tag{26a}$$

$$\mathbb{A}[p_d^\lambda(x)] = \sum_{i=1}^{N} p_d^\lambda(x_i) \cdot [p_d^\lambda(x_i)]^\alpha. \tag{26b}$$

Lemma 2. *Minimizing* $\mathbb{H}[p_d^\lambda(e)]$ *with respect to mass* e_k *requires a positive(negative) update if* $\log e_k$ *is larger(smaller) than* $\mathbb{E}[\log e]$.

Proof. [3]According to the definitions Eqs. equation 26a and equation 25, the entropy can be developed with respect to the probability masses e's as:

$$\mathbb{H}[e] = -\sum_{i=1}^{N} \frac{e_i}{\sum_{j=1}^{N} e_j} \cdot \log\left(\frac{e_i}{\sum_{j=1}^{N} e_j}\right). \tag{27}$$

Based on equation 27, the derivative of $\mathbb{H}[e]$ with respect to the mass e_k can be computed as:

[2]The α hyperparameter is the same used in equation 13

[3]The proof was originally provided by Ji et al. (2021)

$$
\begin{aligned}
\frac{\partial \mathbb{H}}{\partial e_k}[e] &= -\frac{\partial}{\partial e_k}\left(\sum_{i=1}^{N}\frac{e_i}{\sum_{j=1}^{N} e_j}\cdot\log\left(\frac{e_i}{\sum_{j=1}^{N} e_j}\right)\right)\\
&= -\frac{\partial}{\partial e_k}\left(\frac{e_k}{\sum_{j=1}^{N} e_j}\cdot\log\left(\frac{e_k}{\sum_{j=1}^{N} e_j}\right)+\sum_{\substack{i=1\\ i\neq k}}^{N}\frac{e_i}{\sum_{j=1}^{N} e_j}\cdot\log\left(\frac{e_i}{\sum_{j=1}^{N} e_j}\right)\right)\\
&= -\frac{\sum_{j=1}^{N} e_j - e_k}{(\sum_{j=1}^{N} e_j)^2}\log\left(\frac{e_k}{\sum_{j=1}^{N} e_j}\right)-\frac{\sum_{j=1}^{N} e_j - e_k}{(\sum_{j=1}^{N} e_j)^2}-\sum_{\substack{i=1\\ i\neq k}}^{N}\left(\frac{e_i}{(\sum_{j=1}^{N} e_j)^2}\cdot\log\left(\frac{e_i}{\sum_{j=1}^{N} e_j}\right)-\frac{e_i}{(\sum_{j=1}^{N} e_j)^2}\right)\\
&= -\frac{\sum_{\substack{j=1\\ j\neq k}}^{N} e_j}{(\sum_{j=1}^{N} e_j)^2}\log\left(\frac{e_k}{\sum_{j=1}^{N} e_j}\right)-\cancel{\frac{\sum_{\substack{j=1\\ j\neq k}}^{N} e_j}{(\sum_{j=1}^{N} e_j)^2}}-\sum_{\substack{i=1\\ i\neq k}}^{N}\left(\frac{e_i}{(\sum_{j=1}^{N} e_j)^2}\cdot\log\left(\frac{e_i}{\sum_{j=1}^{N} e_j}\right)\right)+\cancel{\frac{\sum_{\substack{i=1\\ i\neq k}}^{N} e_i}{(\sum_{j=1}^{N} e_j)^2}}\\
&= -\sum_{\substack{i=1\\ i\neq k}}^{N}\left(\frac{e_i}{(\sum_{j=1}^{N} e_j)^2}\cdot\log\left(\frac{e_k}{e_i}\right)\right)=\sum_{\substack{i=1\\ i\neq k}}^{N}\left(\frac{e_i}{(\sum_{j=1}^{N} e_j)^2}\cdot\log\left(\frac{e_i}{e_k}\right)\right)\\
&= \sum_{i=1}^{N}\left(\frac{e_i}{(\sum_{j=1}^{N} e_j)^2}\cdot\log\left(\frac{e_i}{e_k}\right)\right)-\cancelto{0}{\frac{e_k}{(\sum_{j=1}^{N} e_j)^2}\cdot\log\left(\frac{e_k}{e_k}\right)}\\
&= \frac{1}{\sum_{j=1}^{N} e_j}\cdot\sum_{i=1}^{N}\left(\frac{e_i}{\sum_{j=1}^{N} e_j}\cdot\log\left(\frac{e_i}{e_k}\right)\right) = \frac{1}{\sum_{j=1}^{N} e_j}\cdot\left(\sum_{i=1}^{N}\left(\frac{e_i}{\sum_{j=1}^{N} e_j}\cdot\log e_i\right)-\log e_k\right).
\end{aligned}
\tag{28}
$$

The update towards minimizing the entropy regularization reads as $e'_k = (e_k - \eta\cdot\frac{\partial\mathbb{H}}{\partial e_k}[e])^+$. According to equation 28, the update $-\eta\cdot\frac{\partial\mathbb{H}}{\partial e_k}[e]$ of mass e_k is positive if $\log e_k$ is larger than $\mathbb{E}[\log e]$ and vice versa. □

Lemma 3. *Minimizing $\mathbb{A}[p_d^\lambda(e)]$ with respect to mass e_k requires a negative(positive) update if e_k^α is larger(smaller) than $\mathbb{E}[e_k^\alpha]$.*

Proof. According to the definitions Eqs. equation 26b and equation 25, the α-order regularization can be developed with respect to the probability masses e's as:

$$
\mathbb{A}[e] = \sum_{i=1}^{N}\frac{e_i}{\sum_{j=1}^{N} e_j}\cdot\left(\frac{e_i}{\sum_{j=1}^{N} e_j}\right)^{\alpha} = \sum_{i=1}^{N}\left(\frac{e_i}{\sum_{j=1}^{N} e_j}\right)^{(\alpha+1)}. \tag{29}
$$

Based on equation 29, the derivative of $\mathbb{A}[e]$ with respect to the mass e_k can be computed as:

$$\frac{\partial \mathbb{A}}{\partial e_k}[e] = \frac{\partial}{\partial e_k}\left(\sum_{i=1}^{N}\left(\frac{e_i}{\sum_{j=1}^{N} e_j}\right)^{(\alpha+1)}\right) = \frac{\partial}{\partial e_k}\left(\left(\frac{e_k}{\sum_{j=1}^{N} e_j}\right)^{(\alpha+1)} + \sum_{\substack{i=1\\ i\neq k}}^{N}\left(\frac{e_i}{\sum_{j=1}^{N} e_j}\right)^{(\alpha+1)}\right)$$
$$= \frac{(\alpha+1)\cdot e_k^{\alpha}\cdot(\sum_{j=1}^{N} e_j)^{(\alpha+1)}}{(\sum_{j=1}^{N} e_j)^{2\cdot(\alpha+1)}} - \frac{(\alpha+1)\cdot e_k^{(\alpha+1)}\cdot(\sum_{j=1}^{N} e_j)^{\alpha}}{(\sum_{j=1}^{N} e_j)^{2\cdot(\alpha+1)}} - \sum_{\substack{i=1\\ i\neq k}}^{N}\left(\frac{(\alpha+1)\cdot e_i^{(\alpha+1)}\cdot(\sum_{j=1}^{N} e_j)^{\alpha}}{(\sum_{j=1}^{N} e_j)^{2\cdot(\alpha+1)}}\right)$$
$$= (a+1)\cdot\left(\frac{e_k^{\alpha}}{(\sum_{j=1}^{N} e_j)^{(\alpha+1)}} - \sum_{i=1}^{N}\left(\frac{e_i^{(\alpha+1)}}{(\sum_{j=1}^{N} e_j)^{(\alpha+2)}}\right)\right) = \frac{(a+1)}{(\sum_{j=1}^{N} e_j)^{(\alpha+1)}}\cdot\left(e_k^{\alpha} - \sum_{i=1}^{N}\left(\frac{e_i}{\sum_{j=1}^{N} e_j}\cdot e_i^{\alpha}\right)\right) \tag{30}$$

Similarly to the entropy minimization case, the update towards minimizing the α-order regularization reads as $e'_k = (e_k - \eta\cdot\frac{\partial\mathbb{A}}{\partial e_k}[e])^+$. According to equation 30, the update $-\eta\cdot\frac{\partial\mathbb{A}}{\partial e_k}[e]$ of mass e_k is negative if e_k^{α} is larger than $\mathbb{E}[e^{\alpha}]$ and vice versa. □

$$d^*(\lambda) \in \arg\min_{d}\left\{\mathrm{KL}[p_{\mathrm{data}}(x)||p_d^{\lambda}(x)] + \gamma\cdot\mathbb{H}[p_d^{\lambda}(x)]\right\}, \tag{24 revisited}$$

Lemma 4. *For $q^* = p_d^{\lambda}(z|x)$, the d^* maximizing the $L_d(\lambda, q^*, d)$ satisfies equation 24.*

Proof. Similar to Theorem 3, we develop the $L_d(\lambda, q, d)$ as:

$$\begin{aligned} L_d(\lambda, q, d) = {} & \mathbb{E}_{p_{\mathrm{data}}}[\log p_{\mathrm{data}}(x)] \\ & - \mathrm{KL}[p_{\mathrm{data}}(x)||p_d^{\lambda}(x)] - \gamma\cdot\mathbb{H}[p_d^{\lambda}(x)] \\ & - \mathbb{E}_{p_{\mathrm{data}}}[\mathrm{KL}[q(z|x)||p_d^{\lambda}(z|x)]] - \gamma\cdot\mathbb{E}_{p_d^{\lambda}}[\mathrm{KL}[q(z|x)||p_d^{\lambda}(z|x)]], \end{aligned} \tag{31}$$

with $\mathbb{H}[\cdot]$ denoting the Shannon entropy. Note that since $\mathrm{KL}[q(z|x)||p_d^{\lambda}(z|x)] \geq 0 = \mathrm{KL}[q^*(z|x)||p_d^{\lambda}(z|x)]$ the d^* maximizing the $L_d(\lambda, q, d)$ can be found as the maximizer of $L_d(\lambda, q^*, d)$. Based on that we set $q = q^*(\lambda, d)$ in 31 and find the d^* that maximizes the objective $L_d(\lambda, q^*(\lambda, d), d)$ as:

$$\begin{aligned} L_d(\lambda, q^*(\lambda, d), d) = {} & \mathbb{E}_{p_{\mathrm{data}}}[\log p_{\mathrm{data}}(x)] \\ & - \mathrm{KL}[p_{\mathrm{data}}(x)||p_d^{\lambda}(x)] - \gamma\cdot\mathbb{H}[p_d^{\lambda}(x)] \\ & - \cancelto{0}{\mathbb{E}_{p_{\mathrm{data}}}[\mathrm{KL}[q^*(z|x)||p_d^{\lambda}(z|x)]]} - \gamma\cdot\cancelto{0}{\mathbb{E}_{p_d}[\mathrm{KL}[q^*(z|x)||p_d^{\lambda}(z|x)]]}. \end{aligned} \tag{32}$$

Based on equation 32, we can derive the maximizer d^* according to equation 24. □

Let us now define:

$$\lambda^*(d) \in \arg\min_{\lambda}\left\{\mathrm{KL}[p_{\mathrm{data}}(x)||p_d^{\lambda}(x)] + \frac{1}{\alpha}\cdot\mathbb{A}[p_d^{\lambda}(x)]\right\}. \tag{33}$$

Lemma 5. *Assuming that $[p_d^{\lambda}(x)]^{\alpha+1} \leq p_{data}(x)$ for all x such that $p_{data}(x) \geq 0$, for $q^* = p_d^{\lambda}(z|x)$, the λ^* maximizing the $L_q(\lambda, q^*, d)$ satisfies equation 33.*

Proof. Given the learnable prior $p_\lambda(z)$ the $L_q(\lambda, q, d)$ becomes:

$$\begin{aligned} L_q(\lambda, q, d) = &\sum_x p_{\text{data}}(x)(\log p_d^\lambda(x) - \text{KL}[q(z|x)||p_d^\lambda(z|x)] \\ &- \frac{1}{\alpha} \cdot [p_d^\lambda(x)]^{\alpha+1} \cdot \exp(-\alpha \cdot \text{KL}[q(z|x)||p_d^\lambda(z|x)])). \end{aligned} \tag{34}$$

Let $q^*(z|x) = p_d^\lambda(z|x)$, the objective $L_q(\lambda, q^*, d)$ reads as:

$$\begin{aligned} L_q(\lambda, q^*, d) &= \sum_x p_{\text{data}}(x) \cdot (\log p_d^\lambda(x) - \cancelto{0}{\text{KL}[q^*(z|x)||p_d^\lambda(z|x)]}) \\ &- \frac{1}{\alpha} \cdot [p_d^\lambda(x)]^{\alpha+1} \cdot \exp(-\alpha \cancelto{1}{\text{KL}[q^*(z|x)||p_d^\lambda(z|x)]}) \\ &= \sum_x p_{\text{data}}(x) \cdot \log p_d^\lambda(x) - \frac{1}{\alpha} \cdot [p_d^\lambda(x)]^{\alpha+1} \\ &= \sum_x p_{\text{data}}(x) \cdot (\log p_d^\lambda(x) - \log p_{\text{data}}(x) + \log p_{\text{data}}(x)) - \frac{1}{\alpha} \cdot [p_d^\lambda(x)]^{\alpha+1} \\ &= \sum_x p_{\text{data}}(x) \cdot \log \frac{p_d^\lambda(x)}{p_{\text{data}}(x)} \\ &+ \sum_x p_{\text{data}}(x) \cdot \log p_{\text{data}}(x) - \frac{1}{\alpha} \cdot \sum_x [p_d^\lambda(x)]^{\alpha+1} \\ &= -\sum_x p_{\text{data}}(x) \cdot \log \frac{p_{\text{data}}(x)}{p_d^\lambda(x)} \\ &+ \sum_x p_{\text{data}}(x) \cdot \log p_{\text{data}}(x) - \frac{1}{\alpha} \cdot \sum_x p_d^\lambda(x) \cdot [p_d^\lambda(x)]^\alpha \\ &= -\text{KL}[p_{\text{data}}(x)||p_d^\lambda(x)] \\ &+ \mathbb{E}_{p_{\text{data}}}[\log p_{\text{data}}(x)] - \frac{1}{\alpha} \cdot \mathbb{A}[p_d^\lambda(x)] \end{aligned} \tag{35}$$

Based on equation 35, we observe that the $\mathbb{E}_{p_{\text{data}}}[\log p_{\text{data}}(x)]$ is fixed given p_{data} while $\mathbb{A}[\cdot]$ is non-negative, therefore we can derive the maximizer λ^* according to 33.

$$d^*(\lambda) \in \arg\min_d \left\{ \text{KL}[p_{\text{data}}(x)||p_d^\lambda(x)] + \gamma \cdot \mathbb{H}[p_d^\lambda(x)] \right\}, \tag{24 revisited}$$

Lemmas 2 and 3 suggest that minimizing the entropy and the α-order push towards the Dirac and uniform distributions respectively. Based on that and the minimization objectives of the d and λ players, we formulate a conjecture on the incompatibility of prior–encoder cooperation.

When training the prior player λ in cooperation with the encoder player q (i.e. to maximize the same $L_q(\lambda, q, d)$ objective), there does not exist λ^* such that the triplet λ^*, q^* satisfiying $q^*(z|x) = p_{d^*}^{\lambda^*}(z|x)$ and d^* as defined in equation 24 constitutes a NE of the game equation 23, under the assumption that $p_{d^*}^{\lambda^*}(x, z) \neq p_{d^*}^{\lambda^*}(x) \cdot p_{d^*}^{\lambda^*}(z)$.

Remark 3. *The Conjecture B.2.1 suggests that the prior–encoder cooperation scheme is not a variable option for prior learning in S-IntroVAE, in the sense that it does not share the same NE with its fixed prior counterpart.*

B.2.2 Prior–decoder Cooperation

Here, we consider the same game defined in equation 23 but under a prior–decoder cooperation scheme where both the prior λ and decoder d players maximize the same objective $L_q(\lambda, q, d)$. First, let us extend Lemma 1 for the learnable prior case.

Lemma 6. *Assuming that* $[p_d^\lambda(x)]^{\alpha+1} \leq p_{data}(x)$ *for all* x *such that* $p_{data}(x) \geq 0$*, the* q^* *maximizing the* $L_q(\lambda, q, d)$ *satisfies* $q^*(\lambda, d)(z|x) = p_d^\lambda(z|x)$*.*

Proof. We develop the $L_q(\lambda, q, d)$ objective as:

$$
\begin{aligned}
L_q(\lambda, q, d) &= \mathbb{E}_{p_{\text{data}}}\left[W(x; \lambda, q, d)\right] - \mathbb{E}_{p_d}\left[\frac{1}{\alpha} \cdot \exp(\alpha \cdot W(x; \lambda, q, d))\right] \\
&= \mathbb{E}_{p_{\text{data}}}\left[\log p_d^\lambda(x) - \text{KL}[q(z|x)||p_d^\lambda(z|x)]\right] \\
&- \frac{1}{a} \cdot \mathbb{E}_{p_d^\lambda}\left[\exp(\log[p_d^\lambda(x)]^\alpha - \alpha \cdot \text{KL}[q(z|x)||p_d^\lambda(z|x)])\right] \\
&= \mathbb{E}_{p_{\text{data}}}\left[\log p_d^\lambda(x) - \text{KL}[q(z|x)||p_d^\lambda(z|x)]\right] \\
&- \frac{1}{a} \cdot \mathbb{E}_{p_d^\lambda}\left[[p_d^\lambda(x)]^\alpha \cdot \exp(-\alpha \cdot \text{KL}[q(z|x)||p_d^\lambda(z|x)])\right] \\
&= \sum_x p_{\text{data}}(x) \cdot (\log p_d^\lambda(x) - \text{KL}[q(z|x)||p_d^\lambda(z|x)]) - \frac{1}{\alpha} \cdot [p_d^\lambda(x)]^{\alpha+1} \cdot \exp(-\alpha \cdot \text{KL}[q(z|x)||p_d^\lambda(z|x)])
\end{aligned}
\tag{36}
$$

We follow the same reasoning used in Lemma 1 and conclude that under the assumption that $[p_d^\lambda(x)]^{\alpha+1} \leq p_{\text{data}}(x)$ holds for all x such that $p_{\text{data}}(x) \geq 0$ $q^*(z|x) = p_d(z|x))$ is the global maxima of the $L_q(q, d)$, that is:

$$
L_q(\lambda, q(\lambda, d), d) \leq L_q(\lambda, q^*(\lambda, d), d) \;\text{ for all }\; q. \tag{37}
$$

□

Let us define λ^* and d^* as:

$$
(\lambda^*, d^*) \in \arg\min_{\lambda, d} \left\{\text{KL}[p_{data}(x)||p_d^\lambda(x)] + \gamma \cdot \mathbb{H}[p_d^\lambda(x)]\right\}. \tag{38}
$$

Now we also modify the Assumption 3 as:

Assumption 4. *For all* x *such that* $p_{data}(x) \geq 0$ *we have that* $[p_{d^*}^{\lambda^*}(x)]^{\alpha+1} \leq p_{data}(x)$*.*

Theorem 4. *Under the Assumption 4, when training the prior player* λ *in cooperation with the decoder player* d *then the triplet* $q^* = p_{d^*}^{\lambda^*}(z|x)$*,* λ^* *and* d^* *as defined in equation 38 constitutes a NE of the game equation 23.*

Proof. Similar to Theorem 3, we develop the $L_d(\lambda, q, d)$ as:

$$
\begin{aligned}
L_d(\lambda, q, d) &= \mathbb{E}_{p_{\text{data}}}[\log p_{\text{data}}(x)] \\
&- \text{KL}[p_{\text{data}}(x)||p_d(x)] - \gamma \cdot \mathbb{H}[p_d(x)] \\
&- \mathbb{E}_{p_{\text{data}}}[\text{KL}[q(z|x)||p_d^\lambda(z|x)]] - \gamma \cdot \mathbb{E}_{p_d^\lambda(}[\text{KL}[q(z|x)||p_d^\lambda((z|x)]],
\end{aligned}
\tag{39}
$$

with $\mathbb{H}[\cdot]$ denoting the Shannon entropy. Note that since $\mathrm{KL}[q(z|x)||p_d^\lambda(z|x)] \geq 0 = \mathrm{KL}[q^*(z|x)||p_d^\lambda(z|x)]$ the (λ^*, d^*) maximizing the $L_d(\lambda, q, d)$ can be found as the maximizer of $L_d(\lambda, q^*, d)$. Based on that we set $q = q^*(\lambda, d)$ in 39 and find the (λ^*, d^*) that maximizes the objective $L_d(\lambda, q^*(\lambda, d), d)$ as:

$$\begin{aligned} L_d(\lambda, q^*(\lambda, d), d) = \mathbb{E}_{p_{\text{data}}}[\log p_{\text{data}}(x)] \\ - \mathrm{KL}[p_{\text{data}}(x)||p_d(x)] - \gamma \cdot \mathbb{H}[p_d(x)] \\ - \cancelto{0}{\mathbb{E}_{p_{\text{data}}}[\mathrm{KL}[q^*(z|x)||p_d(z|x)]]} - \gamma \cdot \cancelto{0}{\mathbb{E}_{p_d}[\mathrm{KL}[q^*(z|x)||p_d(z|x)]]}. \end{aligned} \tag{40}$$

We can now derive the maximizer (λ^*, d^*) according to equation 38. Based on that and according to Lemma 6,

$$\begin{aligned} L_q(\lambda, q(\lambda^*, d^*), d^*) \leq L_q(q^*(\lambda, d^*), d^*) \ \text{ for all } \ q, \\ L_d(\lambda, q^*(\lambda, d), d) \leq L_q(q^*(\lambda^*, d^*), d^*) \ \text{ for all } \ \lambda \text{ and } d, \end{aligned} \tag{41}$$

and therefore we conclude that the triplet λ^*, q^* and d^* such that:

$$\begin{aligned} q^*(z|x) = p_{d^*}^{\lambda^*}(z|x), \\ (\lambda^*, d^*) \in \arg\min_{\lambda, d} \left\{ \mathrm{KL}[p_{\text{data}}(x)||p_d(x)] + \gamma \cdot \mathbb{H}[p_d(x)] \right\}. \end{aligned} \tag{42}$$

is a NE of the equation 23. □

As the proof of the existence of the γ does not assume the nature of the prior, the proof provided by Daniel & Tamar (2021) can be trivially extended for our case of $p_{d^*}^{\lambda^*}$ to show that there exists γ such that the $p_{d^*}^{\lambda^*}$ with (λ^*, d^*) as defined in equation 38 satisfies the Assumption 4.

B.3 Optimal ELBO in the Assumption-free setting

In the previous section, the NE of the S-IntroVAE under the prior–decoder cooperation scheme equation 23 was analyzed under the Assumptions 4. In practice, however, such an assumption might not always be satisfied, particularly in the early stages of training. For instance, it is common in adversarial training for the generator/decoder to generate samples of very low quality (i.e. outside of the support of real data distribution) or to experience mode-collapse (i.e. generating some realistic samples at a disproportionately higher frequency compared to the real data distribution). Evidently, both these cases might lead to violations of said assumption.

Analyzing the behavior of the encoder in the assumption-free setting provides insights into the training dynamics of S-IntroVAE, enabling a better understanding of the method and its relationship to traditional VAEs. Furthermore conducting the analysis with respect to the ELBO $W(x; \lambda, q, d)$ offers a practical tool since the ELBO is comprised of the reconstruction and the KL divergence losses as opposed to the $\mathrm{KL}[q(z|x)||p_d^\lambda(z|x)]$ term (used in Lemma 6) which is intractable.

Let $\mathbb{X} = \{x | x \in p_{\text{data}}(x) > 0 \cup p_d^\lambda(x) > 0\}$, we define the ELBO $W(x; \lambda, q^*, d)$ as:

$$W(x; \lambda, q^*, d) = \begin{cases} -\infty, & x \in \{x \in \mathbb{X} \mid p_{\text{data}}(x) = 0\} \\ \frac{1}{\alpha} \cdot \log \frac{p_{\text{data}}(x)}{p_d^\lambda(x)}, & x \in \{x \in \mathbb{X} \mid p_{\text{data}}(x) > 0 \cap [p_d^\lambda(x)]^{\alpha+1} > p_{\text{data}}(x)\} \\ \log p_d^\lambda(x), & x \in \{x \in \mathbb{X} \mid p_{\text{data}}(x) > 0 \cap [p_d^\lambda(x)]^{\alpha+1} \leq p_{\text{data}}(x)\}\} \end{cases} \tag{43}$$

Proposition 2. *Given a fixed generated data distribution $p_d^\lambda(x)$ the q^* maximizing $L_q(\lambda, d, q)$ in equation 23 is such that the ELBO $W(x; \lambda, q^*, d)$ satisfies 43.*

Proof. Similarly to Lemma 6, we develop $L_q(\lambda, q, d)$ as:

$$
\begin{aligned}
L_q(\lambda, q, d) &= \sum_x p_{\text{data}}(x) \cdot (\log p_d^\lambda(x) - \text{KL}[q(z|x)||p_d^\lambda(z|x)]) - \frac{1}{\alpha} \cdot [p_d^\lambda(x)]^{\alpha+1} \cdot \exp(-\alpha \cdot \text{KL}[q(z|x)||p_d^\lambda(z|x)]) \\
&= \begin{cases} \sum_x p_{\text{data}}(x) \cdot \left(\log p_d^\lambda(x) - \text{KL}[q(z|x)||p_d^\lambda(z|x)] - \frac{1}{\alpha} \cdot \frac{[p_d^\lambda(x)]^{\alpha+1}}{p_{\text{data}}(x)} \cdot \exp(-\alpha \cdot \text{KL}[q(z|x)||p_d^\lambda(z|x)])\right) \\ = \sum_x G(\lambda, q, d), \quad x \in \{p_{\text{data}}(x) > 0\} \\ \\ \sum_x \left(-\frac{1}{\alpha} \cdot [p_d^\lambda(x)]^{\alpha+1} \exp(-\alpha \cdot \text{KL}[q(z|x)||p_d^\lambda(z|x)])\right) \\ = \sum_x Q(\lambda, q, d), \quad x \in \{p_{\text{data}}(x) = 0\} \end{cases}
\end{aligned} \tag{44}
$$

Again, we can find the q^* maximizing $L_q(\lambda, q, d)$ by analyzing the derivatives of the functions $G(\lambda, q, d)$ and $Q(\lambda, q, d)$. In particular, we identify four cases.

- $x \in \{x \in \mathbb{X} \mid p_{\text{data}}(x) > 0 \cap [p_d^\lambda(x)]^{\alpha+1} > p_{\text{data}}(x)\}$

  In this case, the q^* can be found as:

$$
\begin{aligned}
\frac{\partial G(\lambda, q, d)}{\partial \text{KL}[q(z|x)||p_d^\lambda(z|x)]} = 0 \Leftrightarrow \\
p_{\text{data}}(x) \cdot \left(-1 + \frac{[p_d^\lambda(x)]^{a+1}}{p_{\text{data}}(x)} \cdot \exp(-\alpha \cdot \text{KL}[q(z|x)||p_d^\lambda(z|x)])\right) = 0 \Leftrightarrow \\
\exp(-\alpha \cdot \text{KL}[q(z|x)||p_d^\lambda(z|x)]) = \frac{p_{\text{data}}(x)}{[p_d(x)]^{a+1}} \Leftrightarrow \\
-\text{KL}[q(z|x)||p_d^\lambda(z|x)] = \frac{1}{\alpha} \cdot \log \frac{p_{\text{data}}(x)}{[p_d^\lambda(x)]^{a+1}} \Leftrightarrow \\
\log p_d^\lambda(x) - \text{KL}[q(z|x)||p_d^\lambda(z|x)] = \frac{1}{\alpha} \cdot \log \frac{p_{\text{data}}(x)}{[p_d^\lambda(x)]^{a+1}} + \log p_d^\lambda(x) \overset{\text{equation 12}}{\Leftrightarrow} \\
W(x; \lambda, q, d) = \frac{1}{\alpha} \cdot \log \frac{p_{\text{data}}(x)}{[p_d^\lambda(x)]^{a+1}} + \frac{1}{\alpha} \cdot \log [p_d^\lambda(x)]^\alpha \Leftrightarrow \\
W(x; q, d) = \frac{1}{\alpha} \cdot \log \frac{p_{\text{data}}(x)}{p_d^\lambda(x)}.
\end{aligned} \tag{45}
$$

  Note that $\frac{\partial G(\lambda,q,d)}{\partial^2 \text{KL}[q(z|x)||p_d^\lambda(z|x)]} = p_{\text{data}}(x) \cdot \left(-\alpha \cdot \frac{[p_d^\lambda(x)]^{a+1}}{p_{\text{data}}(x)} \cdot \exp(-\alpha \cdot \text{KL}[q(z|x)||p_d^\lambda(z|x)])\right) \leq 0$ therefore the q^* such that $W(x; \lambda, q^*, d) = \frac{1}{\alpha} \cdot \log \frac{p_{\text{data}}(x)}{p_d^\lambda(x)}$ is the maximizer of $L_q(\lambda, q, d)$ for $x \in \{x \in \mathbb{X} \mid p_{\text{data}}(x) > 0 \cap [p_d^\lambda(x)]^{\alpha+1} > p_{\text{data}}(x)\}$.

- $x \in \{x \in \mathbb{X} \mid p_{\text{data}}(x) > 0 \cap [p_d^\lambda(x)]^{\alpha+1} \leq p_{\text{data}}(x)\}$

  In this case, the maximizer of $L_q(\lambda, q, d)$ was found in Lemma 1 as the q^* such that $\text{KL}[q^*(z|x)||p_d^\lambda(z|x)] = 0$. Substracting $\log p_d^\lambda(x)$ to both sides and using equation 12 we get that the q^* such that $W(x; \lambda, q^*, d) = \log p_d^\lambda(x)$ is the maximizer of $L_q(\lambda, q, d)$ for $x \in \{x \in \mathbb{X} \mid p_{\text{data}}(x) > 0 \cap [p_d^\lambda(x)]^{\alpha+1} \leq p_{\text{data}}(x)\}$.

- $x \in \{x \in \mathbb{X} \mid p_{\text{data}}(x) = 0\}$

  In this case, the maximizer of $L_q(\lambda, q, d)$ was found in Lemma 1 as the q^* such that $\text{KL}[q^*(z|x)||p_d^\lambda(z|x)] = \infty$. Substracting $\log p_d^\lambda(x)$ to both sides, using equation 12 and given that $\log p_d^\lambda(x) \leq 0$ we get that the q^* such that $W(x; \lambda, q^*, d) = -\infty$ is the maximizer of $L_q(\lambda, q, d)$ for $x \in \{x \in \mathbb{X} \mid p_{\text{data}}(x) = 0\}$.

- $x \in \{x \in \mathbb{X} \mid p_{\text{data}}(x) = 0 \cap p_d^\lambda(x) = 0\} = \emptyset$

  Note that the $\{p_{\text{data}}(x) = 0 \cap p_d^\lambda(x) = 0\}$ set refers to samples x outside of the support of both real and generated data distributions which are of no practical relevance. In practice, the encoder maximizes the L_q over the expectation of empirical real and generated data distributions, motivating the definition of $\mathbb{X}$ as the union of their supports.

□

Interestingly, the ELBO $W(x; \lambda, q^*, d)$ at the optimal q^* is a continuous function with respect to $p_{\text{data}}(x)$. Additionally, it is revealed that the higher the sample-wise likelihood mismatch between the real $p_{\text{data}}(x)$ and generated $p_d^\lambda(x)$ data distribution, the lower (more negative) the ELBO $W(x; \lambda, q^*, d)$ is. The aforementioned behavior aligns with our intuition as the encoder in S-IntroVAE acts as a discriminator.

On the other hand, given a fixed $p_d^\lambda(x)$, it can trivially shown that the encoder of regularly trained VAEs converges to true posterior which is equivalent to $W_{\text{VAE}}{}^4(x; \lambda, q^*, d) = \log p_d^\lambda(x)$. Naturally, these two observations relate the behavior of the encoders of VAEs and S-IntroVAEs where the latter behaves similarly to the former only if $p_d^\lambda(x)$ is sufficiently "enclosed" by the $p_{\text{data}}(x)$. Given a $p_{\text{data}}(x)$, the "enclosed" term refers to the generated data distribution $p_d^\lambda(x)$ for which the Assumption 3 holds.

The behavior of the Encoder in Practise: Let us now investigate how the theoretical claims suggested the Proposition 2 are realized in practise. For this purpose, the image generation setting was deemed an appropriate testbed due to being easy to interpret while at the same time sufficiently complex allowing us to draw generalizable conclusions. Note that proposition only concerns the optimal encoder given fixed real and generated distributions. Based on that, we employ a well-trained S-IntroVAE and overfit the encoder network while keeping the prior and decoder fixed. In this regard, having the prior and the decoder fixed translates to having a fixed generated data distribution.

As outlined by the proposition, the encoder treats each sample x (i.e. image in this context) differently depending on the likelihood ratio between $p_{\text{data}}(x)$ and $p_d^\lambda(x)$. Unfortunately, to this end, we cannot make use of the Proposition 2 since we do not have access to the analytical densities of either of these distributions. To overcome the aforementioned challenge we use a subset of the real data distribution to construct synthetic real and generated data distributions, denoted as $p_{\text{data}}^{\text{syn}}(x)$ and $p_d^{\lambda^{\text{syn}}}(x)$ respectively. Additionally, it was also necessary, to use a batch size of 1 to avoid leaking information between samples inside and outside of the support of real data distribution due to the batch normalization layers. Based on these synthetic distributions, we can use them as proxies for testing the proposition. Specifically, we experiment with three distinct configurations with different properties: (i) $p_{\text{data}}^{\text{syn}}(x) = p_d^{\lambda^{\text{syn}}}(x)$ where both distributions consist of multiple different samples (ii) $p_{\text{data}}^{\text{syn}}(x)$ consisting of a single sample, whereas $p_d^{\lambda^{\text{syn}}}(x)$ consists of multiple samples, including the single sample from of the $p_{\text{data}}^{\text{syn}}(x)$ and (iii) the reversed (ii) where $p_{\text{data}}^{\text{syn}}(x)$ and $p_d^{\lambda^{\text{syn}}}(x)$ distributions are swapped. We used 10 samples (one for each class) to construct the synthetic distributions.

[4]We used this notation to distinguish it between the ELBO of the S-IntroVAE which we still refer to that simply as W.

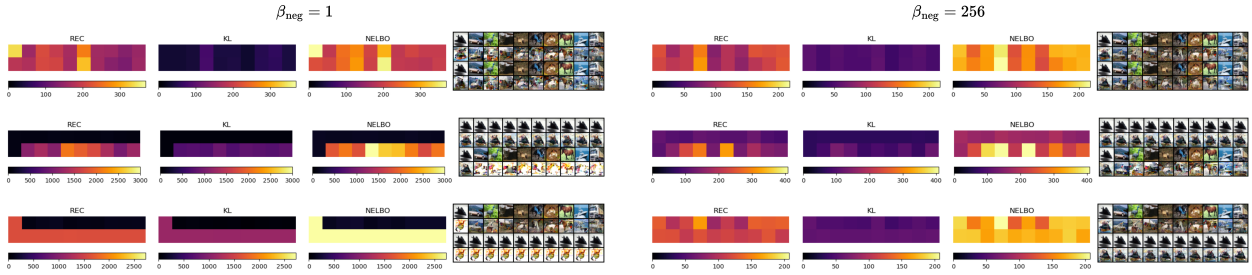

Figure 5: Overfitting the encoder given a fixed generated data distribution across three different configurations (rows). The experiment was conducted both under the theoretically faithful hyperparameter setting ($\beta_{\text{neg}} = 1$ - left) and the one used in praticse ($\beta_{\text{neg}} = 256$ - right). The first line in the REC, KL and NELBO plots refers to the real data distribution whereas the second one refers to the generated data distribution. The images 4^{th} columns correspond to the real data distribution, reconstructed of real data distribution, generated data distribution and reconstructed generated data distribution from top to bottom. The figures above were generated by utilizing a trained S-IntroVAE under a 10-modal MoG prior.

In its theoretical faithful realization the results for (i), (ii) and (iii) are displayed on the left side of Figure 5 under $\beta_{\text{neg}} = 1$. These closely align with what has been suggested by the proposition where when the likelihood of generating a sample is sufficiently enclosed by the likelihood of observing that sample in the real data distribution then the encoder pushes the ELBO towards VAE-optimal levels. On the other hand, in cases where there is a significant likelihood mismatch the encoder can afford to either push the ELBO to its optimal level or diverge from that depending on whether the mismatch appears with respect to the real or the fake data distribution. For instance, when looking at configuration (ii) (2^{nd} row) the encoder minimizes the NELBO (negative ELBO) for the image that is 10 times more likely under the real distribution compared to the fake distribution, whereas the NELBO increases for the samples outside the support of the real data distribution.

In practice, when computing the loss corresponding to maximizing L_q objective, the real and fake ELBOs use different weights for the reconstruction and the KL losses, in particular for CIFAR-10 the β_{neg}, corresponding to the β_{KL} for the fake ELBO, was set to 256 while the remaining $\beta' s$ were set to 1. Using $\beta_{\text{neg}} = 256$ essentially prompts the encoder to focus more on the KL compared to the reconstruction loss when repelling the fake data. However, even in this case, where the hyperparameter configuration diverges from the one theoretically accounted for, we observe that similar patterns emerge.

C Implementation

In this section, we provided the details behind some implementation choices.

C.1 Adaptive Variance Soft-clipping

The (Chang et al., 2023; Chua et al., 2018) works realize log variance soft-clipping as:

$$\begin{aligned} f_c(\text{logvar}) &= \text{logvar} - \text{softplus(logvar-b)} + \text{softplus(a - logvar)} \\ &= \text{logvar} - \frac{1}{\beta} \cdot \log(1 + \exp(\beta \cdot (\text{logvar} - b))) \\ &\quad + \frac{1}{\beta} \cdot \log(1 + \exp(\beta \cdot (a - \text{logvar}))), \end{aligned} \tag{46}$$

where $f_c(\text{logvar})$ is the soft-clipped output, $[a, b]$ is the clipping interval and β a positive hyperparameter controlling the steepness of softplus function. In these works a pre-specified $[a, b]$ range was used and

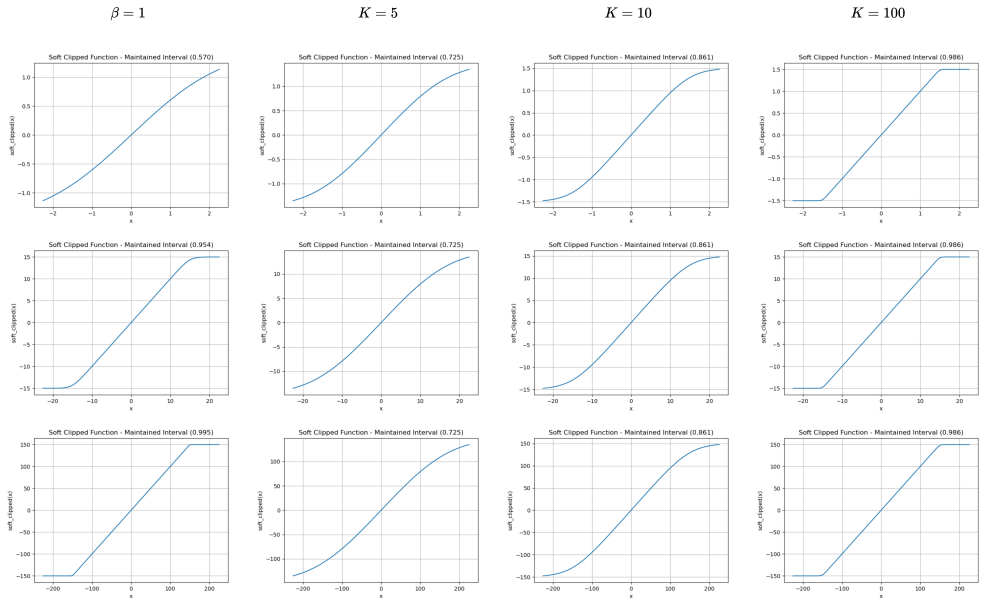

Figure 6: The behavior of soft-clipping depends on the clipping range. Note that when using identical $\beta's$ (e.g. $\beta = 1$) the clipping behavior changes depending on the range (rows). On the other hand, when formulating the β as a function of the range and the K hyperparameter the behavior remains consistent. Increasing the K (columns) leads to retaining a bigger portion of the original clipping range.

naturally finding the optimal β hyperparameter for softplus is subject to proper fine-tuning. In practice, the default option of $\beta = 1$ was used in both studies.

In our case, different clipping intervals are applied to each latent dimension, that is $[a_j, b_j]$ for each j^{th} latent dimension. The $[a_j, b_j]$ interval was determined based on the minimum and maximum variance of the prior's modes in each latent dimension as emerged during the VAE pre-training stage. Based on that, identifying the optimal β_j's through manual fine-tuning is not a feasible option. Towards overcoming this challenge we model the β_j's as:

$$\beta_j = \frac{K}{b_j - a_j}, \tag{47}$$

with K being a controllable hyperparameter. Based on these, we derive the K such that:

$$\frac{f_c(b_j) - f_c(a_j)}{b_j - a_j} \geq \rho, \tag{48}$$

with $\rho \in (0, 1)$. Intuitively the equation 48 suggests that the initial range should be proportionally maintained post the soft-clipping. The maintained proportion is controlled by ρ. Developing equation 48 based on the soft-clipping function defined in equation 46 we get:

$$
\begin{aligned}
f_c(b_j) - f_c(a_j) &\geq \rho \cdot (b_j - a_j) \\
b_j - \frac{1}{\beta_j} \cdot \log(1 + \exp(\beta_j \cdot (b_j - b_j))) + \frac{1}{\beta_j} \cdot \log(1 + \exp(\beta_j \cdot (a_j - b_j))) & \\
-a_i + \frac{1}{\beta_j} \cdot \log(1 + \exp(\beta_j \cdot (a_j - b_j))) - \frac{1}{\beta_j} \cdot \log(1 + \exp(\beta_j \cdot (a_j - a_j))) &\geq \rho \cdot (b_j - a_j) \\
b_i - \frac{1}{\beta_j} \cdot \log(2) + \frac{1}{\beta_j} \cdot \log(1 + \exp(\beta_i \cdot (a_j - b_j))) - a_j + \frac{1}{\beta_j} \cdot \log(1 + \exp(\beta_j \cdot (a_j - b_j))) - \frac{1}{\beta_j} \cdot \log(2) & \\
&\geq \rho \cdot (b_j - a_j) \\
(b_j - a_j) - \frac{2}{\beta_j} \cdot \log(2) + \frac{2}{\beta_j} \cdot \log(1 + \exp(\beta_j \cdot (a_j - b_j))) & \\
&\geq \rho \cdot (b_j - a_j) \\
\beta_j \cdot (1 - \rho) \cdot (b_j - a_j) &\geq \log(4) - 2\log(1 + \exp(\beta_j \cdot (a_j - b_j))).
\end{aligned}
\tag{49}
$$

We can derive K using the formulation defined in *equation* 47 as:

$$
(1 - \rho) \cdot K \geq \log(4) - 2\log(1 + \exp(-K)). \tag{50}
$$

Note that the K only depends on ρ and therefore can be tuned for all latent dimensions simultaneously irrespectively of the soft-clipping range $[a_j, b_j]$ (see Fig. 6). In our study, we used a ρ of 0.85 and found that $K = 10$ satisfies the condition equation 50. In other words, having an adapting $\beta_j = \frac{10}{b_j - a_j}$ guarantees that at least 85% of the initial range is maintained, post-clipping, in all latent dimensions. Alternatively, our β-adapting formulation can be interpreted as a mechanism where the soft-clipping function maintains the same average rate of change in all latent dimensions, as suggested by *equation* 48. Finally, the adaptive clipping function f_c becomes:

$$
\begin{aligned}
f_c(\text{logvar}_j) = \text{logvar}_j &- \frac{1}{\beta_j} \cdot \log(1 + \exp(\beta_j \cdot (\text{logvar}_j - b_j))) \\
&+ \frac{1}{\beta_j} \cdot \log(1 + \exp(\beta_j \cdot (a_j - \text{logvar}_j))).
\end{aligned}
\tag{51}
$$

C.2 Losses in S-IntroVAE with Learnable Prior

Let x_{real} a real sample and $z_\lambda \sim p_\lambda(z)$. The encoder, the decoder, and the prior players minimize the L_E, L_D and L_P losses respectively which write as:

$$
\begin{aligned}
L_E(x_{\text{real}}, \lambda) &= \beta_{\text{rec}} \cdot L_{\text{rec}}(x_{\text{real}}) + \beta_{\text{KL}} \cdot L_{\text{KL}}(x_{\text{real}}) + \frac{1}{\alpha} \cdot \exp(-\alpha \cdot (\beta_{\text{rec}} \cdot L_{\text{rec}}(D(z_\lambda)) + \beta_{\text{neg}} \cdot L_{\text{KL}}(D(z_\lambda)))), \\
L_D(x_{\text{real}}, z_\lambda) &= \beta_{\text{rec}} \cdot L_{\text{rec}}(x_{\text{real}}) + \cancel{\beta_{\text{KL}} \cdot L_{\text{KL}}(x_{\text{real}})} + \gamma \cdot (\gamma_\rho \cdot \beta_{\text{rec}} \cdot L_{\text{rec}}(\texttt{sg}(D(z_\lambda))) + \beta_{\text{KL}} \cdot L_{\text{KL}}(D(z_\lambda))), \\
L_P(x_{\text{real}}, z_\lambda) &= \cancel{\beta_{\text{rec}} \cdot L_{\text{rec}}(x_{\text{real}})} + \beta_{\text{KL}} \cdot L_{\text{KL}}(x_{\text{real}}) + \gamma \cdot (\cancel{\beta_{\text{rec}} \cdot L_{\text{rec}}(\texttt{sg}(D(z_\lambda)))} + \beta_{\text{KL}} \cdot L_{\text{KL}}{}^{5}(D(z_\lambda))),
\end{aligned}
\tag{52}
$$

[5]When computing this particular KL term we only propagate the gradient for prior as a source while applying the `sg` operator for prior as a target.

where $D(z_\lambda)$ is the fake sample generated from decoding the latent z_λ, while L_{rec} and L_{KL} the reconstruction and the KL losses respectively. Both L_E and L_D are identical to the original S-IntroVAE (Daniel & Tamar, 2021) with γ_ρ a hyperparameter also set to $1e^{-8}$. Note that the crossed-out terms do not affect the optimization, as they are constant with respect to the network being updated (e.g., the reconstruction losses are constant with respect to the prior when minimizing the L_P).

C.3 Responsibilities Regularization

In this subsection, we provide the theoretical motivation behind the responsibilities regularization which we utilize to discourage the formation of inactive prior modes. The notion of inactivity describes a prior mode that contributes negligibly in supporting the aggregated posterior compared to other more dominant modes. Sampling from inactive prior modes leads to unconstrained generation, which may negatively impact generation performance. To this end, analyzing the minimization behavior of the $L_{\text{KL}}(x_{\text{real}})$ terms in equation 52 is key to avoiding and/or eliminating the inactive prior modes as these are the terms that induce fitness between the real aggregated posterior and the prior.

Let $q(z|x_s) = \mathcal{N}(z|\mu_s, \sigma_s^2 I)$ be the posterior distribution of the a sample x_s, an M-modal prior distribution $p_\lambda(z) = \sum_{i=1}^{M} w_i \cdot \mathcal{N}(z|\mu_i, \sigma_i^2 I)$ and a uni-modal prior distribution $p_i(z) = \mathcal{N}(z|\mu_i, \sigma_i^2 I)$ corresponding to the i^{th} mode of $p_\lambda(z)$ distribution. Based on these:

$$L_{\text{KL}}(x_s) = \text{KL}[q(z|x_s)||p_\lambda(z)] = \frac{1}{T} \cdot \sum_{t=1}^{T} \log \frac{q(z_s^t|x_s)}{p_\lambda(z_s^t)}, \tag{53}$$

using T MC samples with $z_s^t \sim \mathcal{N}(z|\mu_s, \sigma_s^2 I)$. For simplicity, we now assume that $T = 1$ and drop the index t for notational brevity, that is we refer to the z_s^1 simply as z_s.

C.3.1 Responsibilities Computation - Encoder Update

First, let us analyze the minimization behavior from the encoder's perspective. For a single MC sample z_s, the KL divergence can be computed as:

$$\begin{aligned} \text{KL}[q(z|x_s)||p_\lambda(z)] &= \log q(z_s|x_s) - \log p_\lambda(z_s) \\ &= \log \mathcal{N}(z_s|\mu_s, \sigma_s^2 I) - \log \sum_{i=1}^{M} w_i \cdot \mathcal{N}(z_s|\mu_i, \sigma_i^2 I). \end{aligned} \tag{54}$$

Based on that, we can now compute the derivative of the KL divergence above with respect to z_s as:

$$\begin{aligned} \frac{\partial \text{KL}[q(z|x_s)||p_\lambda(z)]}{\partial z_s} &= \frac{1}{\cancel{\mathcal{N}(z_s|\mu_s, \sigma_s^2 I)}} \cdot \cancel{\mathcal{N}(z^t|\mu_s, \sigma_s^2 I)} \cdot \frac{\mu_s - z_s}{\sigma_s^2} - \sum_{i=1}^{M} \frac{w_i \cdot \mathcal{N}(z_s|\mu_i, \sigma_i^2)}{\sum_{l=1}^{M} w_l \cdot \mathcal{N}(z_s|\mu_l, \sigma_l^2)} \cdot (\frac{\mu_i - z_s}{\sigma_i^2}) \\ &= \frac{\mu_s - z_s}{\sigma_s^2} - \sum_{i=1}^{M} c_i^s \cdot (\frac{\mu_i - z_s}{\sigma_i^2}) \\ &= \cancel{\sum_{i=1}^{M} c_i^s}^{1} \cdot \frac{\mu_s - z_s}{\sigma_s^2} - \sum_{i=1}^{M} c_i^s \cdot (\frac{\mu_i - z_s}{\sigma_i^2}), \end{aligned} \tag{55}$$

with $c_i^s = \frac{w_i \cdot \mathcal{N}(z_s|\mu_i, s_i^2)}{\sum_{l=1}^{M} w_l \cdot \mathcal{N}(z_s|\mu_l, s_l^2)}$ denoting the responsibility of mode i to z_s of the sample x_s.

Similarly we can calculate the derivative of $\mathrm{KL}[q(z|x_s)||p_i(z)]$ with respect to z_s as:

$$\frac{\partial \mathrm{KL}[q(z|x_s)||p_i(z)]}{\partial z_s} = \frac{\mu_s - z_s}{\sigma_s^2} - \frac{\mu_i - z_s}{\sigma_i^2}. \tag{56}$$

Based on Eqs. 55 and 56 we conclude that:

$$\frac{\partial \mathrm{KL}[q(z|x_s)||p_\lambda(z)]}{\partial z_s} = \sum_{i=1}^{M} c_i^s \cdot \frac{\partial \mathrm{KL}[q(z|x_s)||p_i(z)]}{\partial z_s}. \tag{57}$$

The decomposition provided above reveals the effect that responsibilities of each prior component have when fitting uni-modal posterior into multi-modal prior distributions. More specifically, it is shown that z_s minimizes the KL divergence by seeking the prior modes according to the responsibilities c_i^s. Motivated by this, we define the expected responsibility of mode i to the real aggregated posterior as:

$$c_i = \mathbb{E}_{x \sim p_{\mathrm{data}}(x)} \mathbb{E}_{z \sim q_\phi(z|x)} \left[\frac{w_i \cdot \mathcal{N}(z|\mu_i, \sigma_i^2 I)}{\sum_{l=1}^{M} w_l \cdot \mathcal{N}(z|\mu_l, \sigma_l^2 I)} \right]. \tag{58}$$

C.3.2 Inactive Modes and Vanishing Gradients - Prior Update

Let us now compute the derivative of $\mathrm{KL}[q(z|x_s)||p_\lambda(z)]$ with respect to the prior parameters. Similarly to earlier, we compute the KL divergence using a single latent z_s sampled from the posterior distribution of the sample x_s. In this case, the derivative with respect to μ_i and σ_i corresponding to the mean and the standard deviation of the i^{th} prior component respectively, can be computed as:

$$\begin{aligned} \frac{\partial \mathrm{KL}[q(z|x_s)||p_\lambda(z)]}{\partial \mu_i} &= -c_i^s \cdot \frac{z_s - \mu_i}{\sigma_i^2} \text{ and} \\ \frac{\partial \mathrm{KL}[q(z|x_s)||p_\lambda(z)]}{\partial \sigma_i} &= -c_i^s \cdot \frac{(z_s - \mu_i)^2 - \sigma_i^2}{\sigma_i^3}. \end{aligned} \tag{59}$$

When computing the derivative of the KL concerning the contribution w_i we will need to take into account that sum of all contributions has to be 1. To ease the computation we can model $w_i = \frac{e_i}{\sum_{l=1}^{M} e_l}$, where e_i is a non-negative real number realizing the unormalized probability mass of the i^{th} component, and compute the derivative with respect the normalized energy e_i. Based on that :

$$
\begin{aligned}
\frac{\partial \mathrm{KL}[q(z|x_s)||p_\lambda(z)]}{\partial e_i} &= -\frac{\partial \log \sum_{l=1}^{M} w_l \cdot \mathcal{N}(z_s|\mu_l, \sigma_l^2 I)}{\partial e_i} \\
&= -\frac{1}{\sum_{l=1}^{M} w_l \cdot \mathcal{N}(z_s|\mu_l, \sigma_l^2 I)} \cdot \Big(\frac{1}{\sum_{l=1}^{M} e_l} \cdot (1 - w_i) \cdot \mathcal{N}(z_s|\mu_i, \sigma_i^2 I) \\
&\quad - \frac{1}{\sum_{l=1}^{M} e_l} \cdot \sum_{\substack{l=1 \\ l \neq i}}^{M} w_l \cdot \mathcal{N}(z_s|\mu_l, \sigma_l^2 I)\Big) \\
&= -\frac{1}{\cancel{\frac{1}{\sum_{l=1}^{M} e_l}} \cdot \sum_{l=1}^{M} e_i \cdot \mathcal{N}(z_s|\mu_l, \sigma_l^2 I)} \cdot \cancel{\frac{1}{\sum_{l=1}^{M} e_l}} \cdot \Big(\mathcal{N}(z_s|\mu_i, \sigma_i^2 I) \\
&\quad - \sum_{l=1}^{M} w_l \cdot \mathcal{N}(z_s|\mu_l, \sigma_l^2 I)\Big) \\
&= \frac{1}{\sum_{l=1}^{M} e_i \cdot \mathcal{N}(z_s|\mu_l, \sigma_l^2 I)} \cdot \Big(\sum_{l=1}^{M} w_l \cdot \mathcal{N}(z_s|\mu_l, \sigma_l^2 I) - \mathcal{N}(z_s|\mu_i, \sigma_i^2 I)\Big).
\end{aligned} \tag{60}
$$

The result above aligns with our intuition as it suggests that given a latent z_s the energy e_i corresponding to the unnormalized contribution of i^{th} component increases if it is more likely to have been sampled from that mode compared to the MoG prior, and vice versa.

The derivatives above reveal the behavior of the individual prior components in the presence of inactive modes. In particular, an inactive mode i manifests as low c_i responsibility (i.e., c_i^s close to zero for all real sample x_s), due to insufficiently supporting the real aggregated posterior relative to other, more dominant modes. Consequently, a vanishing gradient issue arises, where the mean and the standard deviation of the inactive mode i are not updated (towards supporting the posterior) as indicated by 59. On the other hand, the unnormalized contributions of the inactive modes tend to vanish in favor of other more dominant modes as Eq 60 suggests. Based on these observations, it is clear that in the presence of inactive modes, allowing for learnable contributions enables the prior player to eliminate inactive modes. Conversely, not allowing learnable contributions leaves the prior with inactive modes that cannot adapt to the aggregated posterior, due to their low responsibility and consequently vanished gradients rendering the model prone to unconstrained generation.

D Additional Details and Results

D.1 Baseline Reproduction for 2D Datasets

Due to the inherent randomness involved in evaluating the generation quality, the grid-search-based hyperparameter tuning and the computation of KL-divergence in a Monte-Carlo fashion, in table 4 we compare the baseline performance across five key settings. Namely, the baseline as (i) reported in (Daniel & Tamar, 2021) (ii) reproduced by us using the official code-base (Daniel & Tamar, 2021), reproduced by our code-base computing KL both (iii) in closed-form (c) and (iv) in Monte-Carlo (s) manner and finally (v) replicated by our full pipeline of hyperparameter tuning which can result in selecting different optimal hyperparameter for each dataset (compared to those provided by Daniel & Tamar (2021)). Although computing the KL divergence in a Monte-Carlo fashion is unnecessary for the uni-modal prior (baseline) it is important to verify that both closed and Monte-Carlo-based KL computation lead to comparable performance.

2D - Dataset	β_{rec}	β_{kl}	β_{neg}
8Gaussian	0.2 (0.2)	0.3 (0.3)	0.9 (0.9)
2Spirals	0.2 (0.2)	0.05 (0.5)	0.2 (1)
Checkerboard	0.05 (0.2)	0.2 (0.1)	0.8 (0.2)
Rings	0.2 (0.2)	0.2 (0.2)	0.6 (1)

Table 3: Optimal hyperparameter under the standard Gaussian prior for each dataset as found using grid-search and as reported by Daniel & Tamar (2021) (in parenthesis).

		S-IntroVAE (standard Gaussian)				
		reported	official (reproduced)	ours (reproduced)		ours (replicated)
KL calculation		c	c	c	s	s
8Gaussian	gnELBO ↓	1.25 ±0.35	0.62 ±0.13	0.52 ±0.09	**0.51 ±0.15**	**0.51 ±0.15**
	KL ↓	1.25 ±0.11	1.33 ±0.52	1.36 ±0.41	**1.23 ±0.11**	**1.23 ±0.11**
	JSD ↓	**0.96 ±0.15**	1.16 ±0.15	1.16 ±0.11	1.01 ±0.18	1.01 ±0.18
2Spirals	gnELBO ↓	**5.21 ±0.04**	5.47 ± 0.05	5.47 ± 0.06	5.47 ±0.14	6.41 ±0.61
	KL ↓	**8.13 ±0.3**	10.21 ±0.39	10.66 ±0.19	10.26 ±0.39	9.5 ±1.23
	JSD ↓	**3.37 ±0.04**	4.03 ±0.1	4.11 ±0.16	4.08 ±0.06	4.21 ±0.5
Checkerboard	gnELBO ↓	**4.47 ±0.29**	6.28 ±0.56	6.22 ±0.80	6.33 ±0.75	7.21 ±0.12
	KL ↓	20.27 ±0.21	19.72 ±0.23	19.99 ±0.28	19.94 ±0.37	**19.62 ±0.57**
	JSD ↓	9.06 ±0.15	9.04 ±0.19	9.34 ±0.19	9.19 ±0.17	**8.87 ±0.15**
Rings	gnELBO ↓	6.3 ±0.08	5.81 ±0.06	**5.8 ±0.05**	5.85 ±0.13	6.03 ±0.12
	KL ↓	**9.18 ±0.33**	10.67 ±0.5	10.75 ±0.29	10.89 ±0.45	9.99 ±0.59
	JSD ↓	4.13 ±0.09	4.37 ±0.12	4.35 ±0.12	4.2 ±0.11	**4.05 ±0.15**

Table 4: Baseline performance across five key settings. For each setting, we report the performance across 5 seeds. When reporting the performance for columns 2 to 4 we used the optimal hyperparameters as provided (reproduced) by Daniel & Tamar (2021) (also found in parenthesis in Table 3) whereas, for the 5$^{\text{th}}$ column, we used the optimal hyperparameters found by our grid-search implementation (replicated). Note that for the 8Gaussian dataset, we found the same optimal hyperparameters leading to identical performance between the 4$^{\text{th}}$ and the 5$^{\text{th}}$ columns. The 'c' and 's' refer to closed-form and sample-based computation of KL divergence.

D.2 MoG Ablation on the Image Experiments

In Table 5 we provide the full ablation on the image generation benchmark suggesting that utilizing a sufficient number of prior modes is crucial for achieving optimal generation and representation learning performance.

		S-IntroVAE								
		SG	VAMP(10) → MoG(10)				VAMP(100) → MoG(100)			
	LC	✗	✗	✗	✓	✓	✗	✗	✓	✓
	IP	✗	✗	✓	✗	✓	✗	✓	✗	✓
MNIST	r_{entropy}	0	10	0	1	100	10	10	1	10
	Entr.	0	0.966 ±0.013	0.952 ±0.024	0.948 ±0.016	0.988 ±0.002	0.892 ±0.003	0.882 ±0.003	0.882 ±0.004	0.853 ±0.007
	FID (GEN) ↓	1.414 ±0.044	1.38 ±0.085	1.356 ±0.173	1.427 ±0.034	1.365 ±0.054	1.322 ±0.044	1.352 ±0.09	1.32 ±0.105	**1.309 ±0.046**
	FID (REC) ↓	1.503 ±0.053	1.488 ±0.124	1.51 ±0.085	1.629 ±0.297	1.472 ±0.120	**1.342 ±0.087**	1.473 ±0.174	1.363 ±0.13	1.385 ±0.141
	SVM (few) ↑	0.93 ±0.002	0.956 ±0.003	**0.972 ±0.002**	0.957 ±0.004	0.959 ±0.004	0.961 ±0.002	0.97 ±0.007	0.962 ±0.003	**0.972 ±0.003**
	SVM (many) ↑	0.93 ±0.002	0.957 ±0.003	**0.972 ±0.002**	0.957 ±0.003	0.958 ±0.004	0.961 ±0.002	0.97 ±0.007	0.962 ±0.003	**0.972 ±0.003**
	KNN (few) ↑	0.763 ±0.005	0.866 ±0.017	0.943 ±0.009	0.876 ±0.012	0.842 ±0.024	0.916 ±0.007	0.947 ±0.019	0.92 ±0.002	**0.957 ±0.007**
	KNN (many) ↑	0.87 ±0.006	0.897 ±0.017	0.949 ±0.01	0.907 ±0.01	0.885 ±0.015	0.934 ±0.004	0.953 ±0.013	0.935 ±0.002	**0.958 ±0.004**
FMNIST	r_{entropy}	0	10	10	0	1	0	10	10	10
	Entr.	0	0.978 ±0.006	0.982 ±0.001	0.951 ±0.011	0.82 ±0.041	0.931 ±0.005	0.931 ±0.002	0.944 ±0.001	0.903 ±0.009
	FID (GEN) ↓	3.326 ±0.067	2.778 ±0.155	3.019 ±0.165	2.836 ±0.154	2.987 ±0.124	2.785 ±0.088	3.025 ±0.241	**2.727 ±0.137**	2.831 ±0.173
	FID (REC) ↓	3.76 ±0.168	3.102 ±0.107	3.406 ±0.062	3.189 ±0.159	3.339 ±0.14	**2.994** ±0.087	3.129 ±0.165	3.185 ±0.175	3.511 ±0.128
	SVM (few) ↑	0.681 ±0.002	0.703 ±0.019	0.681 ±0.018	0.715 ±0.009	0.68 ±0.021	**0.731 ±0.005**	0.695 ±0.011	0.712 ±0.009	0.696 ±0.004
	SVM (many) ↑	0.731 ±0.011	0.771 ±0.008	0.763 ±0.011	0.775 ±0.005	0.765 ±0.003	**0.78 ±0.003**	0.772 ±0.005	0.778 ±0.003	0.773 ±0.004
	KNN (few) ↑	0.425 ±0.016	0.594 ±0.027	0.649 ±0.021	0.604 ±0.025	0.618 ±0.023	0.683 ±0.011	0.693 ±0.014	0.678 ±0.01	**0.707 ±0.009**
	KNN (many) ↑	0.606 ±0.024	0.682 ±0.024	0.691 ±0.013	0.69 ±0.018	0.659 ±0.015	0.736 ±0.006	0.729 ±0.01	0.731 ±0.006	**0.739 ±0.007**
CIFAR-10	r_{entropy}	0	10	10	10	0	10	100	100	10
	Entr.	0	0.895 ±0.008	0.886 ±0.01	0.914 ±0.021	0.0	0.839 ±0.012	0.94 ±0.004	0.929 ±0.006	0.511 ±0.074
	FID (GEN) ↓	4.424 ±0.11	4.538 ±0.172	4.876 ±0.13	4.547 ±0.136	4.595 ±0.08	4.465 ±0.066	**4.385 ±0.242**	4.417 ±0.054	4.594 ±0.407
	FID (REC) ↓	4.13 ±0.119	4.379 ±0.092	4.686 ±0.248	4.539 ±0.16	4.519 ±0.102	4.205 ±0.157	**4.084 ±0.011**	4.141 ±0.068	4.585 ±0.645
	SVM (few) ↑	0.245 ±0.015	0.241 ±0.008	0.264 ±0.009	0.246 ±0.017	0.224 ±0.005	0.25 ±0.003	**0.271 ±0.011**	0.26 ±0.003	0.256 ±0.005
	SVM (many) ↑	0.391±0.009	0.385 ±0.006	0.379 ±0.003	0.387 ±0.003	0.365 ±0.004	0.396 ±0.004	**0.407 ±0.013**	0.401 ±0.003	0.396 ±0.003
	KNN (few) ↑	0.206 ±0.002	0.175 ±0.004	0.238 ±0.007	0.175 ±0.004	0.174 ±0.007	0.189 ±0	**0.239 ±0.009**	0.196 ±0.002	0.219 ±0.004
	KNN (many) ↑	0.308 ±0.012	0.192 ±0.016	0.305 ±0.002	0.186 ±0.008	0.219 ±0.028	0.216 ±0.015	**0.32 ±0.009**	0.259 ±0.005	0.273 ±0.008

Table 5: Quantitative performance on the images datasets. The r_{entropy} row corresponds to the regularization used to obtain the optimal FID(GEN) for each training configuration, where the Entr. row refers to the normalized entropy of the responsibilities where the closer to one its value the more uniformly the aggregated posterior is supported by the prior components.

D.3 Illustrating the Effect of Regularizing the Entropy of the Responsibilities.

Regularizing the entropy of the responsibilities, as described in C.3, was essential for avoiding the formation of inactive modes in our prior–decoder cooperation scheme. Here we provide empirical evidence for that choice by analyzing the curves of normalized entropy of the responsibilities for different regularization intensities controlled by the r_{entropy} hyperparameter and the corresponding FID(GEN) measuring the generation quality. Towards identifying the optimal value we experimented with $r_{\text{entropy}} \in [0, 1, 10, 100]$, however, to enhance the readability of Fig. 7, we omitted the curves for $r_{\text{entropy}} = 1$ as they displayed similar behavior to $r_{\text{entropy}} = 0$.

Inspecting Fig. 7 reveals interesting insights into the effect of responsibilities' regularization. First, it can be seen that different optimal r_{entropy} are to be expected depending on the prior learning configuration and the datasets as indicated by the FID(curves). Additionally, we observe that the issue of inactive prior mode formation is more pronounced under the IP formulation. The blue lines, representing unregularized responsibilities, tend to converge to a lower level compared to the fixed MoG prior setting. We attribute this behavior to the prior modes being updated to support the aggregated posterior, which adapts according to a discriminating objective. Interestingly, we also observe that when allowing for learnable contribution (i.e. LC) under the IP generally decreases the entropy of the responsibilities. This observation can be explained by the derivative of KL with respect to the energy contributions as given by Eq 60. More specifically it was shown that the contributions of inactive prior modes tend to decrease in favor of more dominant ones, further reducing the normalized entropy of the responsibilities. Finally, the FID(GEN) curves corresponding to CIFAR-10 dataset highlight the detrimental effect of generating samples from inactive modes. More specifically, when the responsibilities' entropy approaches zero (blue curves in CIFAR-10) the FID(GEN) tends to increase when not allowing for learnable contributions (dotted blue curves). In other words, generating samples from modes that do not support the aggregated posterior (i.e., inactive modes) leads to degraded generation quality.

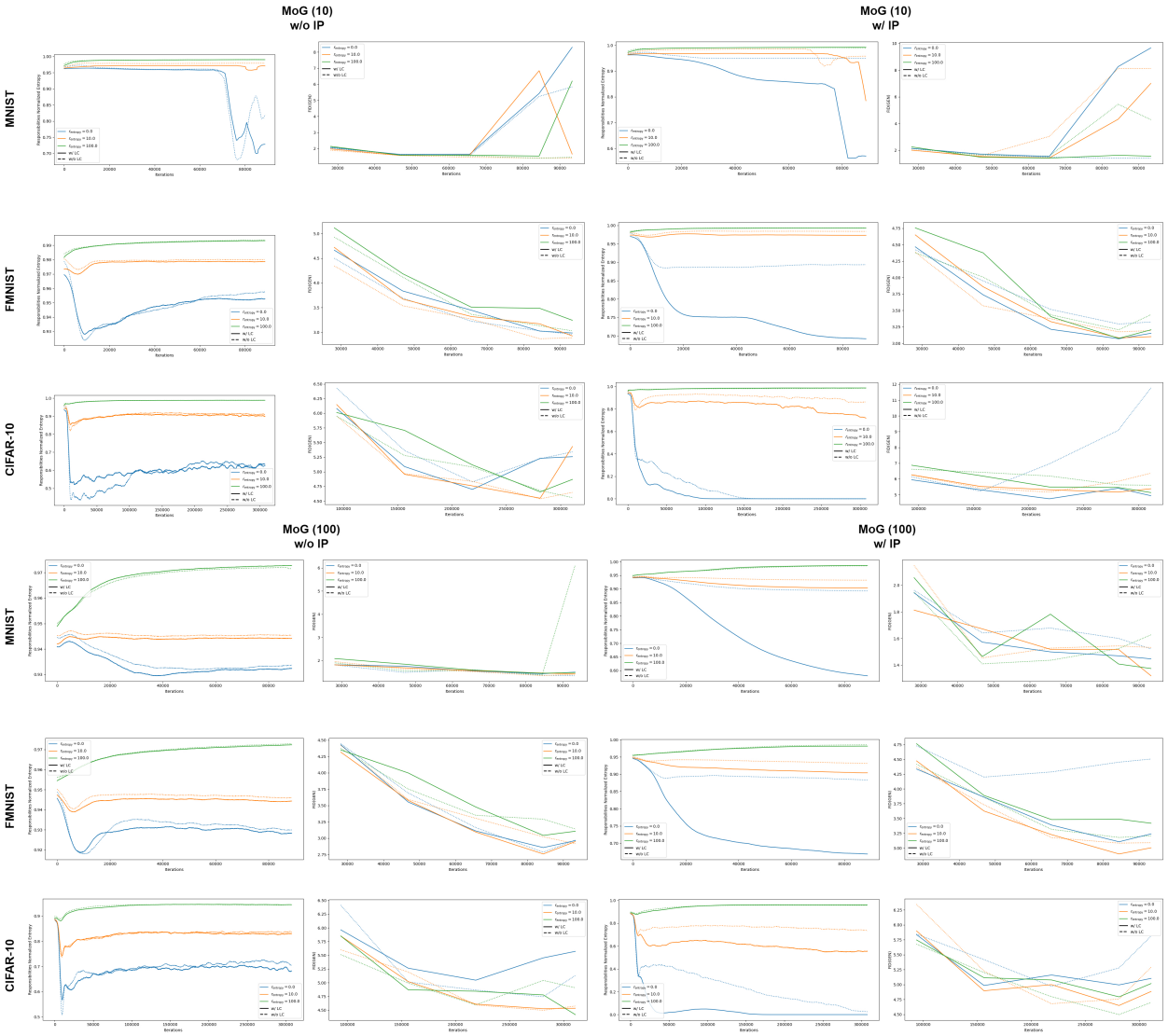

Figure 7: The effect of regularizing the entropy of the responsibilities under the 10− and 100−modal MoG priors.

D.4 Latent Space Inspection

Here, we provide visualizations of the latent space of S-IntroVAE under the different configurations considered for the image generation task. More specifically we are interested in understanding how allowing for a learnable prior affects the latent space learned in S-IntroVAEs. Overall, the quantitative results suggest that learning the prior during the adversarial training leads to significantly different latent space. In particular, we observe that the prior components are spread more evenly when allowing for learnable prior compared to when fixing it (see Fig. 8).

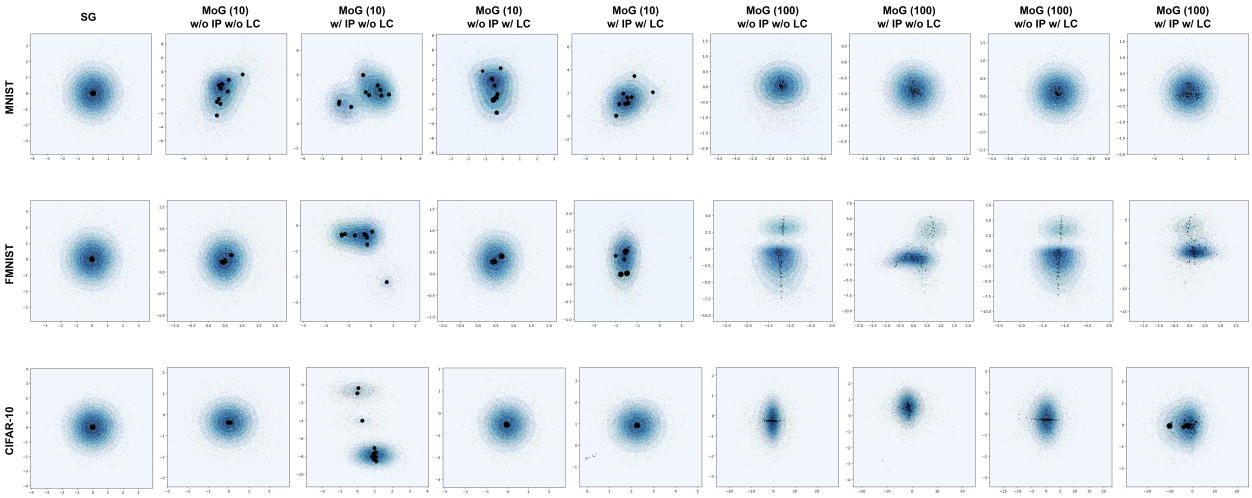

Figure 8: Visualizing the first 2 latent dimensions of S-IntroVAE under different prior configurations along with samples from the aggregated posterior. Different colors correspond to different classes. Note that learning the prior during the adversarial learning leads to significantly different latent space. The black dots refer to the means of the prior components, when applicable (i.e. w/ LC) the size of these dots refers to the contribution of this component in the MoG (e.g. the smaller the size the lower the contribution).

We also employed the t-SNE dimensionality reduction technique to visually inspect how prior learning affects the high-dimensional latent space. The quantitative results indicate that prior learning tends to create better-separated clusters. Although the separation effect is less pronounced when modeling the prior with many components (e.g. 100 vs 10 components), it remains noticeable (see Fig. 9).

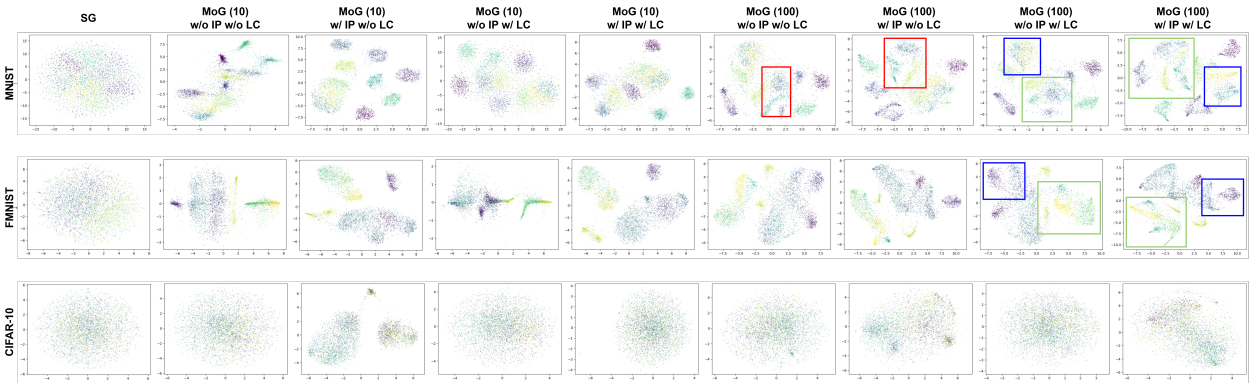

Figure 9: Visualizing the high-dimensional latent space of the aggregated posterior using t-SNE dimensionality reduction technique. Note that learning the prior during the adversarial learning generally leads to better-separated clusters in the latent space. Different colors correspond to different classes.